

The High-Z Supernova Search: Measuring Cosmic Deceleration and Global Curvature of the Universe Using Type Ia Supernovae¹

(To appear in the Astrophysical Journal)

Brian P. Schmidt², Nicholas B. Suntzeff³, M. M. Phillips³, Robert A. Schommer³,
Alejandro Clocchiatti^{3,4}, Robert P. Kirshner⁵, Peter Garnavich⁵, Peter Challis⁵, B.
Leibundgut⁶, J. Spyromilio⁶, Adam G. Riess^{5,7}, Alexei V. Filippenko⁷, Mario Hamuy⁸, R.
Chris Smith^{4,9}, Craig Hogan¹⁰, Christopher Stubbs¹⁰, Alan Diercks¹⁰, David Reiss¹⁰, Ron
Gilliland¹¹, John Tonry¹², José Maza¹³, A. Dressler¹⁴, J. Walsh⁶, and R. Ciardullo¹⁵

¹This work is based in part on observations at the European Southern Observatory, La Silla, Chile.

Received _____; accepted _____

²Mount Stromlo and Siding Spring Observatories, Private Bag, Weston Creek P.O., ACT 2611, Australia.

³Cerro Tololo Inter-American Observatory, Casilla 603, La Serena, Chile; National Optical Astronomy Observatories, operated by the Association of Universities for Research in Astronomy, Inc. (AURA), under cooperative agreement with the National Science Foundation.

⁴Current Address: Departamento de Astronomia y Astrofisica, Pontificia Universidad Catolica de Chile, Casilla 104, Santiago 22, Chile

⁵Harvard-Smithsonian Center for Astrophysics, 60 Garden St., Cambridge, MA 02138.

⁶European Southern Observatory, Karl-Schwarzschild-Strasse 2, D-85748 Garching, Germany.

⁷Department of Astronomy, University of California, Berkeley, CA 94720-3411.

⁸Steward Observatory, University of Arizona, Tucson, AZ 85721.

⁹University of Michigan, Department of Astronomy, 834 Dennison, Ann Arbor, MI 48109-1090.

¹⁰Department of Astronomy, University of Washington, Seattle, WA 98195-1580.

¹¹Space Telescope Science Institute, 3700 San Martin Drive, Baltimore, MD 21218.

¹²Institute for Astronomy, University of Hawaii, Manoa, Honolulu, HI 96822.

¹³Departamento Astronomía, Universidad de Chile, Casilla 36-D, Santiago, Chile.

¹⁴Carnegie Observatories, 813 Santa Barbara Street, Pasadena, CA 91101.

¹⁵Pennsylvania State University, Department of Astronomy & Astrophysics, 525 Davey Laboratory, University Park, PA 16802.

ABSTRACT

The High-Z Supernova Search is an international collaboration to discover and monitor type Ia supernovae (SN Ia) at $z > 0.2$ with the aim of measuring cosmic deceleration and global curvature. Our collaboration has pursued a basic understanding of supernovae in the nearby Universe, discovering and observing a large sample of objects, and developing methods to measure accurate distances with SN Ia. This paper describes the extension of this program to $z \geq 0.2$, outlining our search techniques and follow-up program. We have devised high-throughput filters which provide accurate two-color restframe B and V light curves of SN Ia, enabling us to produce precise, extinction-corrected luminosity distances in the range $0.25 < z < 0.55$. Sources of systematic error from K-corrections, extinction, selection effects, and evolution are investigated, and their effects estimated. We present photometric and spectral observations of SN 1995K, our program's first supernova, and use the data to obtain a precise measurement of the luminosity distance to the $z = 0.479$ host galaxy. This object, when combined with a nearby sample of SN, yields an estimate for the matter density of the Universe of $\Omega_M = -0.2^{+1.0}_{-0.8}$ if $\Omega_\Lambda = 0$. For a spatially flat universe composed of normal matter and a cosmological constant, we find $\Omega_M = 0.4^{+0.5}_{-0.4}$, $\Omega_\Lambda = 0.6^{+0.4}_{-0.5}$. We demonstrate that with a sample of ~ 30 objects, we should be able to determine relative luminosity distances over the range $0 < z < 0.5$ with sufficient precision to measure Ω_M with an uncertainty of ± 0.2 .

Subject headings: cosmology: observations — galaxies: distances and redshifts — supernovae: general — supernovae: individual (SN 1995K)

1. Introduction

Measuring the cosmological parameters which describe the global properties of the Universe has been a fundamental quest in astronomy ever since Robertson (1936) and Walker (1936) formulated the metric for a homogeneous and isotropic Universe. By observing how a standard candle dims as a function of redshift, usually shown as a Hubble diagram, the effects of curvature and cosmic deceleration can be observed and quantified (Sandage 1961). Early luminosity distance investigations (Humason, Mayall, & Sandage 1956; Baum 1957; Minkowski 1960) used brightest cluster galaxies as standard candles and measured galaxy brightnesses in the range $0.01 < z < 0.5$. Attempts to trace luminosity distances versus redshifts with these galaxies at $z > 0.1$ changed emphasis when it was realized both from theory (Tinsley 1972) and observation (e.g., Oke, Gunn, & Hoessel 1996) that the effects of galaxy evolution are much larger than the differences due to cosmology.

Although many other methods for measuring the global curvature and cosmic deceleration exist (e.g., Peebles 1993), none has yet delivered a definitive result. For example, measuring the number of galaxies as a function of magnitude maps out the volume of space as a function of redshift, and can be used to gauge the global geometry. Attempts to use this method (Shanks et al. 1984) have been hampered by galaxy evolution and merging, although some of the uncertainty may be eliminated by moving to the infrared (Yoshi & Peterson 1995). Another test examines the angular size of a standard rod as a function of redshift. Kellerman (1993) resolved a large sample of compact radio sources out to $z \approx 3$ using Very Long Baseline Interferometry. Although the angular sizes increase at $z > 1$ as expected for a non-empty Universe, evolutionary effects are hard to quantify. Stepanas & Saha (1995) have also shown that the unknown intrinsic distribution of source sizes makes it difficult to obtain a statistically significant measurement of cosmological parameters. Guerra & Daly (1998) have also used extended radio galaxies as standard rods

and show that the results are consistent with a low density universe.

Type Ia supernovae (SN Ia) have long been considered promising tools for measuring extragalactic luminosity distances, but only recent searches, the resulting sets of light curves and spectra, and new methods of analysis (Phillips 1993 [P93]; Hamuy et al. 1995, 1996a-d [H95,H96a-d]; Riess, Press, & Kirshner 1995, 1996a [RPK95, RPK96]) have quantified the nature, power, and limitations of SN Ia as distance indicators. SN Ia offer high intrinsic luminosity [$M_B \approx -19.4$ mag (Saha et al. 1997)] and as individual stars, may not be subject to the same evolutionary effects which plague galaxies (although this must be demonstrated). Even before this breakthrough in understanding SN Ia, two searches for distant SN Ia were initiated (Nørgaard-Nielsen et al. 1989; Perlmutter et al. 1995) to measure cosmological parameters. These searches demonstrate that it is possible to find SN at $z > 0.3$ with large-format CCD detectors, and give hope that a significant sample of SN Ia can be gathered in just a few years. Perlmutter et al. (1997, 1998) have already presented observations of 8 objects at $z > 0.35$. A sample of ~ 30 objects, if carefully measured and shrewdly analyzed, will provide a statistically interesting measurement of global cosmological parameters.

Recently, much effort has been put into examining how to use the power spectrum of fluctuations in the cosmic microwave background (CMB) to measure cosmological parameters (see Hu 1996 for a review). Future satellite missions, such as the Microwave Anisotropy Probe and Planck Missions, will measure temperature fluctuations across the sky on scales substantially less than a degree, determining the power spectrum of fluctuations out to a multipole expansion of $\ell > 500$. Model fits to these observations promise to provide simultaneous measurement of ten cosmological parameters. However, because the fits are degenerate for certain combinations of interesting parameters such as Ω_M and Ω_Λ , the CMB observations will need to be combined with other observational

data, such as those from high-redshift supernovae (Zaldarriaga, Spergel, & Seljak 1997), to determine Ω_M and Ω_Λ individually.

This paper reports on the High-Z SN Search, a coordinated program to discover, spectroscopically classify, and measure photometrically in at least two filters a distant set of SN Ia. This enterprise aims to measure the deceleration parameter, q_0 , with an uncertainty smaller than 0.1, and will place strong limits on combinations of cosmological parameters such as $\Omega_M - \Omega_\Lambda$. The CMB observations provide a nearly orthogonal set of parameters, so we will be able to separate the effects of any exotic forms of matter-energy in the Universe from normal matter. We will be able to discern whether the Universe is open, closed, or has nearly zero global curvature. Preliminary results from our program were reported by Schmidt et al. (1996), Schmidt (1997), and Leibundgut & Spyromilio (1997). In addition, we have confirmed the predicted time-dilation of redshifted objects using SN Ia light curves (Leibundgut et al. 1996) and spectra (Riess et al. 1997), and presented observations of 3 objects observed with *HST* (Garnavich et al. 1998).

In §2 we describe how the expansion, deceleration, and curvature of the Universe are related to luminosity distances, and in §3 we discuss measuring distances with SN Ia at $z < 0.1$. Our supernova search and observational follow-up program are outlined in §4. In §5 we present the techniques and limitations of using SN Ia to measure accurate luminosity distances at $z > 0.2$. Observations of the first SN discovered by this program, SN 1995K at $z=0.479$, are presented in §6, with the techniques discussed in §3-5 applied to this object. We summarize the High-Z SN Search to date in §7 and use the results for SN 1995K to estimate the precision with which we will be able to constrain cosmological parameters.

2. Expansion, Deceleration, and Curvature

The precise large-scale isotropy of the microwave background confirms a picture in which the Universe is accurately described on large scales by the maximally symmetric, Robertson-Walker line element (e.g., Weinberg 1972). For events with time separation dt , radial coordinate separation dr , and angular separation $d\theta$, the line element ds is given by

$$ds^2 = dt^2 - a^2(t) \left[\frac{dr^2}{1 - kr^2} + r^2 d\theta^2 \right]. \quad (1)$$

The global spatial geometry has the character of a hypersphere of radius $k^{-1/2}a(t)$, where $a(t)$ is the cosmic scale factor which defines the physical scale of the hypersphere at each time. In these units the spatial curvature parameter k can be 1, 0, or -1 , corresponding to a closed, flat, or open Universe, respectively.

The complete spacetime metric, which depends on $a(t)$, is determined by the Friedmann equation

$$H^2 \equiv (\dot{a}/a)^2 = \frac{8\pi G\rho}{3} - \frac{k}{a^2}, \quad (2)$$

where ρ is the total density of all forms of matter-energy. Friedmann-Robertson-Walker (FRW) cosmologies are based on equations (1) and (2), and provide a complete description of an isotropic and homogeneous universe.

We adopt a conventional model in which the matter content of the Universe is composed of a sum of components each having a fraction Ω_i of the current critical density $\rho_{crit} \equiv 3H_0^2/8\pi G$ and various equations of state with density $\rho_i \propto (\text{volume})^{-(1+\alpha_i)}$ [e.g., $\alpha = 0$ for normal matter (Ω_M), $\alpha = -1$ for a cosmological constant (Ω_Λ), $\alpha = +1/3$ for radiation (Ω_{rad}), $\alpha = -1/3$ for non-commuting strings (Ω_S)]. It is convenient to adopt a parameter $\kappa_0 \equiv kc^2/[a(t_0)^2 H_0^2]$ representing the scalar curvature in units commensurate with the density parameters; the current physical radius of hypersphere curvature is $k^{-1/2}a(t_0) = \kappa_0^{-1/2}cH_0^{-1}$ and the definition of critical density gives $\kappa_0 = \sum_i \Omega_i - 1$. We can

then write the Friedmann equation in terms of these model parameters,

$$H^2 = H_0^2 \left[\sum_i \Omega_i (1+z)^{3+3\alpha_i} - \kappa_0 (1+z)^2 \right]. \quad (3)$$

It is conventional to define a “deceleration parameter” $q_0 \equiv -\ddot{a}(t_0)a(t_0)/\dot{a}^2(t_0)$, characterizing the low-redshift behavior, which can be expressed as

$$q_0 = \frac{1}{2} \sum_i \Omega_i (3 + 3\alpha_i) - \sum_i \Omega_i = \frac{1}{2} \sum_i \Omega_i (1 + 3\alpha_i). \quad (4)$$

Distance measurements based on SN Ia light curves are described as luminosity distances, D_L , and are defined by the ratio of the intrinsic luminosity \mathcal{L} to the observed flux \mathcal{F} as

$$D_L = \left(\frac{\mathcal{L}}{4\pi\mathcal{F}} \right)^{\frac{1}{2}}. \quad (5)$$

In FRW cosmologies D_L is derived by computing the area of the sphere over which the flux is distributed from a source at a radial coordinate fixed by the redshift. Including the effects of time dilation and redshift, the luminosity distance is

$$D_L H_0 = (1+z) |\kappa_0|^{-1/2} S\{|\kappa_0|^{1/2} \int_0^z dz' [\sum_i \Omega_i (1+z')^{3+3\alpha_i} - \kappa_0 (1+z')^2]^{-1/2}\}, \quad (6)$$

where $S\{x\} \equiv \sin(x)$, x , or $\sinh(x)$ for $k = 1, 0, -1$, respectively (Coles & Lucchin 1995).

Mattig (1958) showed that when normal matter is the only contributor to Ω ,

$$D_L H_0 = \frac{1}{q_0^2} \left[q_0 z + (q_0 - 1) (\sqrt{1 + 2q_0 z} - 1) \right]. \quad (7)$$

Alternatively, equation (6) can be expanded in z to give

$$D_L H_0 = z + z^2 \left(\frac{1 - q_0}{2} \right) + \mathcal{O}(z^3), \quad (8)$$

which is valid for all models. The linear term of the expansion is the Hubble law, and has been studied for many years. Its linear form has been verified to high precision in the nearby Universe using SN Ia with the same techniques we employ for this project (H96b;

RPK96; Tammann & Leibundgut 1990), using brightest cluster galaxies (Lauer & Postman 1992), and again using SN Ia at larger redshifts (Kim et al. 1997). The current debate on the value of H_0 centers on obtaining an absolute calibration for these distance indicators in nearby galaxies through accurate absolute distances. The measurements of curvature and deceleration require only a relative distance indicator to obtain the shape of the (D_L, z) relation, and are not affected by current uncertainties in H_0 due to local calibration. Equation (8) shows that departures in the luminosity distance from a pure Hubble law, to lowest order in z , are proportional to q_0 — they depend only on deceleration and not on curvature. With a distance modulus, $m - M = 5 \log_{10}(D_L/10 \text{ parsec})$, measured to precision Δm mag for an object at redshift z , equation (8) shows (using $\Delta m = 5\Delta \log_{10}[H_0 D_L]$) that we measure q_0 to a precision $\Delta q_0 \approx 0.9\Delta m/z$; thus a single well-observed SN Ia at $z = 0.5$ with $\sigma = 0.15$ mag (H96b, RPK96) should yield a precision of about $\Delta q_0 = 0.27$, almost a 2σ discrimination between an empty ($q_0 = 0$) and a flat ($q_0 = 0.5$) Universe. However, we caution the reader that already at $z = 0.5$, $\mathcal{O}(z^3)$ terms cannot be neglected, especially in cosmologies with significant cosmological constants.

To illustrate the precise effects of cosmology on luminosity distance, we plot the differences in distance modulus, $m - M$, from an $\Omega_{\text{tot}} = 0$ Universe as a function of redshift for a set of universes composed of different amounts and types of matter-energy (Figure 1). Although first order deviations constrain only the linear combination of parameters corresponding to deceleration, data on objects over a range of redshifts up to $z \approx 1$ can separate out the effects of the various forms of mass-energy in the (D_L, z) relation, and place limits on global curvature. In particular, it is possible to separate flat cosmological models with non-zero Ω_Λ from open universes containing only normal matter (Goobar and Perlmutter 1995).

3. Using Type Ia Supernovae to Measure Luminosity Distances

SN Ia have been used as extragalactic distance indicators since Kowal (1968) published a Hubble diagram ($\sigma = 0.6$ mag) for SN I. We now recognize that the old SN I spectroscopic class conflated two distinct types of objects: SN Ib/c which are probably massive stars that undergo core collapse after losing their hydrogen atmospheres, and SN Ia which are most likely thermonuclear explosions of white dwarfs (see Filippenko 1997 for a review). Modern versions of the SN I (now SN Ia) Hubble diagram shows scatter about the inverse-square line of about 0.3 to 0.5 mag (Tammann & Leibundgut 1990; van den Bergh & Pazder 1992; Branch & Miller 1993; Sandage & Tammann 1993), which is remarkable given the heterogeneous sources and oftentimes poor observations upon which these diagrams are based.

The advent of precise observations of nearby SN Ia made with CCD detectors produced evidence for genuine differences in the luminosities, light curve shapes, and spectra among the Type Ia family. SN 1984A (Branch 1987; Barbon, Rosino, & Iijima 1989), SN 1986G (Phillips et al. 1987), SN 1991bg (Filippenko et al. 1992b; Leibundgut et al. 1993), and SN 1991T (Filippenko et al. 1992a; Phillips et al. 1992) provided proof that SN Ia were not all identical objects whose observed differences could be attributed to measurement errors, but that real differences among these explosions are undoubtedly present.

The problem of understanding SN Ia well enough to use them as cosmological probes despite their intrinsic variation was solved by assembling a sufficiently large, uniform, and well-observed data set. In 1990 a group of astronomers at CTIO and the University of Chile at Cerro Calán initiated a systematic photographic search for SN Ia using the Curtis Schmidt telescope at CTIO (Hamuy et al. 1993a). Their program, which discovered 30 SN Ia in 2.5 years, also acquired high-quality spectral and photometric follow-up for these supernovae. The resulting data set (H96c) allows the precise determination of the properties

of SN Ia as distance indicators. At maximum light, SN Ia have an intrinsic range of > 2 mag in B and > 1 mag in V . Although this is an interesting result for supernova physics, it does not bode well for using SN Ia as high-precision distance indicators without additional information.

Although their brightness at maximum light has a moderately large scatter, SN Ia do exhibit a correlation ($\sigma \approx 0.15$ mag) between the rate at which their luminosity declines and absolute magnitude. P93 demonstrated this relationship by plotting the absolute magnitude of ten nearby SN Ia which had dense photoelectric or CCD coverage, versus the parameter $\Delta m_{15}(B)$, the amount by which the SN decreased in brightness in the B band over the 15 days following maximum light. The sample showed a correlation, which when taken into account, dramatically improved the predictive power of SN Ia. The Calán/Tololo survey yielded an independent confirmation of the P93 absolute magnitude-decline rate relationship from the sample of 30 SN Ia by using a χ^2 fitting technique to the B, V , and I light curves (H95, H96a). When corrected for their rate of decline, H96c demonstrated that the scatter in the Hubble diagram could be lowered to $\sigma \sim 0.15$ mag in V for a sample of nearly 30 SN Ia. Another technique, the Multicolor Light Curve Shape (MLCS) method, has been developed by RPK95 and RPK96. By “training” on a nearby set of objects (P93’s sample plus a few additions), they achieve $\sigma < 0.2$ mag on a sample of 20 objects (H95, augmented by 10 additional well observed SN Ia) in the Hubble flow. This result is encouraging because the Hubble diagram derived by RPK96 is independent of the objects on which their method was “trained,” and therefore provides an upper limit for the true dispersion of this distance measuring technique. Other methods to correct for intrinsic luminosity differences or limits on the input sample by various criteria have also been proposed to increase the precision of SN Ia as distance indicators (Tammann & Sandage 1995; Fisher et al. 1995; van den Bergh 1995; Branch et al. 1996; Perlmutter et al. 1997).

The analyses described above assume that all SNe Ia can accurately be described by a one-parameter family of light curves. We know this is not true because the scatter about the Hubble line in either H96c and RPK96 is larger than the observational errors would indicate (H96c,RPK96). The inferred scatter beyond the observational uncertainties is small, ($\sigma \approx 0.12$ mag), and the residuals (including observational uncertainties) are distributed about the mean with a distribution consistent with a Gaussian. To this date, no other observable has been shown to successfully account for the remaining small intrinsic scatter about the one parameter family of light curves. Unless supernovae are much different at high redshift, the imperfection of SN Ia as distance indicators will have a negligible impact on using SN Ia as cosmological probes.

4. Search and Follow-Up Program

Many techniques have been successfully used to discover supernovae, including visual observations of nearby galaxies (Evans 1994), photographic surveys (Zwicky 1968; Mueller 1989, McNaught 1990, Hamuy et al. 1993a; Pollas 1992), and CCD surveys (Perlmutter et al. 1992, 1995; Treffers et al. 1993; Martin, Williams, & Woodings 1997; Reiss et al. 1998). Although it is possible to discover objects up to $z \approx 1$ (Schmidt et al. 1997c) by using large format CCDs coupled with wide fields on telescopes with the best image quality, it is efficient to measure cosmological parameters by observing objects in the range $0.35 < z < 0.55$. When systematic effects are small, the leverage gained with high-redshift objects is offset by the difficulty in obtaining accurate measurements. It is challenging to obtain accurate restframe B and V photometry of objects observed at $0.55 < z < 0.9$ because they are outside the optimum K-correction window (Figure 2), and these SN are currently less powerful tools for measuring cosmological parameters than their lower redshift siblings. The *Hubble Space Telescope* (*HST*) + WFPC2/NICMOS could acquire accurate

restframe B and V measurements for SN Ia at $z \approx 1$. These objects hold the promise of establishing powerful constraints on cosmology within this more distant observational window. From the ground, however, the band $0.35 < z < 0.55$ gives the best combination of measurements and systematics to investigate cosmology.

4.1. Observing Strategy

To maximize the number of SN Ia discovered in our target redshift range, $0.35 < z < 0.55$, we observe a large area and aim to achieve a limiting magnitude of $m_R \approx 23$ mag, which is ~ 1 magnitude fainter than the expected brightness of a $z = 0.5$ SN Ia at maximum light (Figure 4). Finding objects is not the only consideration; the objects must be found near or before maximum light, and we need to follow discoveries with spectra and multi-color photometry. To ensure our objects are discovered young, we use the technique described by Hamuy et al. (1993a) and Perlmutter et al. (1995), imaging fields near the end of a dark run, and then reimaging the fields at the beginning of the next dark run. These two runs, separated by approximately 21 days (close to the rise time of a time-dilated SN Ia at $z=0.5$), provide objects which are at, or before maximum light¹⁶. Observations are generally made near the celestial equator, so that we can use telescopes in both hemispheres for follow-up spectroscopy and photometry. At least two observations are made at each search position, to detect motion of asteroids, eliminate cosmic rays, and remove chip defects.

As an outgrowth of this project, Riess et al. (1997) developed a method to measure the age of a SN Ia relative to maximum light from its spectrum alone. This technique is

¹⁶To target objects in the other advantageous K-correction window, $z \approx 1$, observations to $m_I = 24$ mag, separated by 30 days, will efficiently deliver young SN Ia.

especially valuable because it provides another way to identify young objects, ideally while still observing at the telescope.

Since we need to schedule large blocks of telescope time months in advance to follow the supernovae, it is essential to have candidates after each supernova discovery run, and not be derailed by weather. During the summer months of December through March, the Chilean Atacama desert has nearly 100% clear weather. We have concentrated our search efforts at the CTIO 4 m telescope, the instrument which currently provides the widest field of view of any large telescope in Chile.

On the CTIO 4 m telescope we image approximately 3 square degrees per night with a single 2048^2 detector, taking two consecutive 150 s $B45$ exposures of each field. In good conditions ($1''$ seeing), a combined frame has a limiting magnitude of $m_R \approx 23$, and provides a sufficiently long time baseline to remove Kuiper belt objects, which have a typical parallax motion of $3'' \text{ hr}^{-1}$. Since January 1997, the “Big Throughput Camera” (BTC) has been available at the CTIO 4 m telescope. This mosaic of 4 chips quadruples the imaging area, but has a somewhat longer readout time. We have recently used the BTC to obtain two consecutive 300s R exposures at every pointing, enabling us to cover 7 square degrees per night to a depth of $m_R = 23.5$ mag.

4.2. Search Software

Our supernova search is automated, with final cuts on potential candidates being made by eye. The automated processing program is written in PERL, and calls IRAF tasks, DoPHOT (Schechter, Mateo, & Saha 1993), and various programs written in C. In brief, the program aligns the second-epoch image with the first, initially finding the bright stars using DoPHOT, and then matching stars in the two frames using a triangle-matching algorithm

similar to that described by Groth (1986). The images are then registered using the IRAF tasks “geomap” and “geotran.” After registration, we match the point spread functions (PSF) of the two epochs applying the method of Phillips & Davis (1995), which computes a convolution kernel in Fourier space, and fits the high frequencies with a Gaussian profile. The DoPHOT analytic PSF measurements show which image needs to be degraded, and indicates if the PSF matching cannot be made in a single convolution. This is the case when the images are elongated with respect to each other such that neither image has a FWHM which is smaller than the other at all position angles. In these cases, we convolve one of the images with an appropriate Gaussian, and then apply the Phillips & Davis method. After PSF matching, the images are scaled to the same intensity and sky brightness values by plotting the intensity of each pixel in one image against the intensity of the corresponding pixel in the other in a subraster centered on a star. We fit for an offset (difference in sky brightness) and a scale (differential atmospheric transparency), and then subtract the intensity-scaled images. This procedure is carried out on both second-epoch images, and these differenced images are averaged, rejecting any high pixels which are discordant by more than 3σ .

The resulting image is searched using a point-source detection algorithm. Our algorithm samples the combined difference image at many locations over the image, estimating the average noise within a PSF, and then scans the image for objects above this threshold by a certain number of σ ($\sigma > 4$ being a typical choice). A list of candidates, eliminating those near known bright stars, is sorted by magnitude. This entire process takes about 6 minutes to run on a 170 MHz Sun UltraSparc for a pair of 2048^2 images. For inspection of candidates, the examiner is presented with subrasters of the candidate’s region from the first epoch, both second epochs, and the subtracted image. These images can be viewed simultaneously as a mosaic, or stacked and blinked.

The number of candidates to examine depends on the detection threshold and the quality of the match between the two epochs. Typically, 5-50 objects are examined on each pair of search images, but most are easily eliminated by inspection. Our approach is to minimize false alarms from a night of observing. We usually have 5–20 possible SN candidates per night that are detected by our software filter and which are not discarded by visual inspection. When there is doubt about the reality of a candidate, we make a repeat observation of the field. At this point, the candidate list is sent to collaborators for spectroscopic observations that can show whether or not the object is a supernova, give some information on its type and age, and provide the redshift. Roughly 75% of these candidates are confirmed as SN Ia, the remainder consisting of other supernova types, AGNs, and occasional mystery objects. These mystery objects typically have no visible host galaxy, and fade by more than two magnitudes within 24 hours (and in one case, at least 2 magnitudes in 3 hours). It is conceivable that these are flare stars in the halo of the Milky Way, or the unbeamed optical counterparts to gamma-ray bursts (Rhoads 1997). There is no bias in our selection against SN in which there is no visible galaxy since the whole CCD field is searched.

4.3. Data Reduction Procedures

We extract the high-redshift photometry in the same way we have measured the $z < 0.1$ sample (H96c, RPK96). We first calibrate a local photometric sequence of stars which appear in the CCD field of each supernova. These stars are calibrated by observing standard stars on photometric nights, deriving color and atmospheric extinction transformations, and then applying these to the local sequence. The local photometric sequence, which typically spans a substantial range of color and brightness, is then combined, correcting for any color term of the system used in the observation, with relative photometry between

the supernova and sequence stars to produce a standard magnitude for the supernova. In general, the color terms of our different systems are small, since most of the supernova observations are taken with identical filters as described in Appendix A.

To produce precise relative photometry for our high-redshift supernovae we follow the same procedure employed in the Calán/Tololo survey for galaxy subtraction (Hamuy et al. 1994). A template image, in which the supernova is absent, is required for every object/filter combination. Ideally, these images would have better seeing than any of the other observations, so that the observations are not degraded in the PSF matching process, and should have more than twice the signal-to-noise (S/N) ratio to minimize the addition of shot noise in the subtractions. In most cases images of our SN discovery regions which are appropriate for use as templates are not in hand before the time of explosion, so we must return to these fields after about a year to obtain templates. One of our most difficult tasks is to obtain good seeing images with long integration times to serve as acceptable templates. The analysis of our edata set will be continuously improved as we build up improved templates for the supernovae we follow.

We have developed a pipeline closely related to our search software for extracting photometry from our CCD frames. After normal processing in which the frames are bias subtracted and flat fielded, this pipeline uses the search software to align an image to the template, match the two images' PSFs, scale the intensity of the observation to the template, and then subtract the template from the observation in a region around the galaxy. The software then runs DoPHOT on the galaxy-subtracted frame, using a fixed position of the supernova¹⁷ and a sequence of comparison stars, to extract the magnitude of the supernova. After measuring the SN's brightness, the script builds a PSF from the

¹⁷In low S/N ratio situations, allowing the centroid of the PSF to be a free parameter would cause a systematic over-estimate of the object's flux.

comparison stars using DAOPHOT (Stetson 1987), and adds this PSF to user specified galaxies in the image so that they have the same brightness as the SN measurement. After subtracting the template from the areas containing the added PSFs, DoPHOT is once again run to extract the magnitudes of these artificial SN. These synthetic objects provide an effective method to estimate the relative photometric errors, and can give a strong indication if something has gone wrong in the reduction process.

Our spectra are reduced in a typical manner, except that we generally extract only a small region along the slit at the position of the supernova to minimize host galaxy contamination. We also bin the spectra as necessary in the dispersion direction, after final reduction, to increase the S/N ratio per pixel, to aid in classifying the objects.

5. Measuring Accurate Relative Distances Between Nearby and High-Z SN Ia

The distances derived to SN Ia are well characterized and tested in the nearby Universe, but accurately comparing these objects to their more distant counterparts requires great care. Selection effects can introduce systematic errors as a function of redshift, as can uncertain K-corrections, or an evolution of the SN Ia progenitor population as a function of look-back time. These effects, if they are large, will limit our ability to measure the (D_L, z) relation accurately, and have the potential to sap the potency of high-redshift SN Ia for measuring cosmological parameters.

5.1. Extinction

Most attempts at using SN Ia as distance indicators have not corrected for extinction in the supernova host galaxy. The majority of the SN Ia discovered at $z < 0.1$ which comprise the current sample of well observed SN Ia have been detected using photography

at Schmidt telescopes, and it is possible that many SN Ia embedded in dusty spiral arms or galaxy nuclei were missed by these searches. Distant SN Ia are discovered with CCD observations by subtracting a digital template from the data, and are more affected by galaxy surface brightness than galaxy morphology. Additional complications arise because magnitude-limited selection might prevent extinguished objects from being discovered with equal efficiency in both nearby and distant samples, or because the smaller angular size of distant objects makes it more difficult to detect SN deep inside spirals — those likely to be extinguished. In short, it would not be surprising to have systematic differences between the average extinctions of objects discovered in the nearby and distant supernova searches. Rather than attempt to untangle this hopelessly knotted set of selection effects, we believe it is more straightforward to correct for extinction of individual objects that are in the samples based on their colors.

Except for a small group of very rapidly fading supernovae, H95 show that SN Ia have a relatively small range in their $(B - V)$ color at maximum light which can be used to estimate their extinction. Even so, it is worthwhile to correct for extinction according to the prescription of P93/H95 or RPK95. Using the framework set out earlier in this section, but for two filters, a relative reddening estimate of any SN Ia can be extracted from its observations, by simultaneously fitting B and V (or any set of two or more photometric bands) and deriving the $E(B - V)$ offset. This procedure does not require the training set to be free of reddening, as the calculated color excess will be relative to the average extinction of the training set. In practice, using an iterative process, it is possible to define an essentially reddening-free set of synthetic light curves, weeding out the reddened objects on the basis of their color evolution. RPK96 have demonstrated that using B, V, R , and I light curves within their framework, dispersions of less than 0.15 mag are attainable. Furthermore, they show that their best estimate of the reddening law from a few heavily reddened objects in their sample of SN Ia is indistinguishable from the mean Galactic

reddening law (Riess, Press, & Kirshner 1996b). A recent study by Phillips et al. (1998) based on previous work by Lira (1996) on the intrinsic color evolution of SN Ia has also developed a consistent method to deredden type Ia light curves. Correcting SN Ia for extinction does not necessarily decrease their dispersion as distance indicators (extinction corrections only decrease the scatter when the error in the derived extinction is less than the dispersion caused by extinction to a sample of objects), but is essential to remove the systematic bias that absorption might introduce.

It is possible that the average properties of dust might evolve as a function of look-back time, e.g., the LMC and SMC have extinction laws which differ significantly from that of the Milky Way (Bouchet et al. 1985). Such an effect could significantly bias the comparison of nearby and distant objects if the average extinction to either the nearby or distant sample is large. Although the nearby sample of objects has few reddened objects (RPK96), and indications are that the high- z sample has low extinction as well (Riess et al. 1998), this possible bias warrants further investigation. For example, observations of reddened objects in rest-frame BVR_CI_C at large redshifts could be used to investigate the extinction law at these look-back times, and limit uncertainties introduced by this effect.

5.2. K-corrections

When comparing objects at significant redshifts with nearby counterparts, it is necessary to account for the wavelength shift of light. The effect of redshift on luminosity distances, dubbed the K-correction, was tabulated for galaxies in modern photometric bands by Oke & Sandage (1968). They defined the K-correction K_i such that an object's magnitude m_i in filter i as a function of redshift z is

$$m_i(z) = m_i(z = 0) + K_i(z). \quad (9)$$

An object with spectrum $F(\lambda)$ (in units of power per unit area per unit wavelength) observed in a filter with sensitivity function $S_i(\lambda)$ has

$$m_i(z = 0) = -2.5 \log \frac{\int S_i(\lambda) F(\lambda) d\lambda}{\int S_i(\lambda) d\lambda} + \mathcal{Z}_i, \quad (10)$$

where \mathcal{Z}_i is the zero point of the filter¹⁸. Oke & Sandage demonstrated that

$$K_i = 2.5 \log \left[(1+z) \frac{\int F(\lambda) S_i(\lambda) d\lambda}{\int F(\lambda/(1+z)) S_i(\lambda) d\lambda} \right], \quad (11)$$

where K_i accounts for the $(1+z)$ shift of the photons in wavelength, and the $(1+z)$ increase in the unit $d\lambda$ which they occupy. In the case of SN Ia, K-corrections have an added complication caused by the changing spectral energy distribution of a supernova as it evolves. SN Ia change rapidly when they are near maximum, which translates to rapidly changing (and hence uncertain) K-corrections (Hamuy et al. 1993). This evolution is particularly pronounced blueward of 4000 Å due to line blanketing, and therefore using K-corrections in the traditional manner on the observed B and V light curves of SN Ia at $z = 0.5$ is an extremely risky proposition. Following the precepts of Gunn (1978), Perlmutter et al. (1995) demonstrated that by observing distant SN Ia with the R_C broadband filter, K-correction uncertainties could be substantially reduced, because at $z = 0.5$ the R_C filter approximates the restframe B filter. Kim, Goobar, & Perlmutter (1996) show that this modified K-correction is

$$K_{ij} = 2.5 \log \left[(1+z) \frac{\int F(\lambda) S_i(\lambda) d\lambda}{\int F(\lambda/(1+z)) S_j(\lambda) d\lambda} \right] + \mathcal{Z}_j - \mathcal{Z}_i, \quad (12)$$

where $K_{ij}(z)$ is the correction for going from filter i to filter j . Note that if filter i is exactly the redshifted counterpart of filter j , then at this redshift K_{ij} is not zero, but has a constant

¹⁸Traditionally \mathcal{Z}_i has been set such that when equation (10) is applied to the spectrum of Vega, it yields $m_i = 0.03$ mag. However, many photometric systems have \mathcal{Z}_i which vary slightly from this definition.

value corresponding to the $(1 + z)$ stretching of the wavelength region $d\lambda$ photons occupy combined with the difference in the zero points of the filters.

Rather than constrain ourselves to existing broadband filter sets, we decided to define our own set of redshifted filters, created as broadband interference filters. We currently have defined four filters — pairs of B and V filters redshifted to $z = 0.35$ and $z = 0.45$ (henceforth referred to as the $B35$, $V35$, $B45$, and $V45$ filters). Although adopting this new photometric system adds the complication of defining standards for these filters, we believe the ability to translate SN Ia observed in the range $0.25 < z < 0.55$ to standard B and V filters with small systematic and statistical uncertainties makes it worthwhile. An overview of our system is given in Appendix A.

An important advantage in designing new filters is that modern transmission coatings have peak transmissions in excess of 85%, whereas traditional R_C and I_C filters are typically around 60%. In addition, our filters have a sharp cut-off on the long wavelength side, which results in significantly lower backgrounds from night sky lines than their Kron-Cousins counterparts. In Figure 2 we have plotted the uncertainty in the K-corrections in translating to restframe B and V from both our specialized filters (Appendix A), the R_C and I_C filters (Bessell 1990), and selected *HST* filters. These corrections have been calculated using the series of SN Ia spectra in Hamuy et al. (1993b), augmented with additional spectra of SN 1994D by Filippenko (1997). The resulting K-corrections are fit as a function of SN age for each redshift with a low-order polynomial, and the residual scatter of this fit is used to gauge the uncertainty of the K-corrections. The estimated uncertainties are insensitive to the exact order of the polynomial used, and provide an estimate of the random component of K-correction uncertainties due to errors in our SN Ia spectrophotometry and intrinsic differences in supernovae. For proper redshift-filter matches, the resulting K-corrections in transforming to restframe B and V are accurate to better than 3% for

SN Ia observed between 14 days before maximum and 50 days past maximum over the range of $0.25 < z < 0.55$ (and using *HST*, between $0.90 < z < 1.1$). For objects which are extinguished, it is necessary to modify the spectra used for determining the K-corrections iteratively with reddening curves, using fits to their light curves to estimate the amount of extinction. In addition, if the SN differs significantly from those used to construct the K-corrections, a substantial error can result, especially when the object is at a redshift where the filter is not a close match to its restframe counterpart. In these cases, the first order difference between the spectra is usually color, and the spectra used for determining the K-corrections can be adjusted with a power law to match the color evolution of the object. The systematic uncertainty in translating between filter systems limits the accuracy with which we are able to measure luminosity distances at high redshift. Note that K-correction zero point errors are magnified through extinction corrections: since $A_V = 3.1E(B - V)$, a 0.02 mag uncertainty of $(B - V)$ translates to a 0.06 mag uncertainty in distance modulus. It is a very difficult task to ensure systematic errors in $(B - V) < 0.02$ mag in either the nearby or distant sample, and we believe that this uncertainty will be our largest source of systematic error.

5.3. Evolution

An attractive feature of using SN Ia as distance indicators at significant redshifts is the possibility of minimizing the evolutionary effects which plague distance indicators based on the properties of galaxies. Initial models proposed that SN Ia arise from the explosions of carbon-oxygen white dwarfs as they reach the Chandrasekhar mass (Hoyle & Fowler 1960; Arnett 1969; Colgate & McKee 1969). This mechanism for SN Ia explosions leads to a burning front which propagates outwards from the white dwarf's center, burning nearly the entire star to nuclear statistical equilibrium. A broader range of models for the

presupernova star and for the behavior of the burning wave is needed to account for the intermediate-mass elements that are seen in the spectra of SN Ia (Wheeler & Harkness 1990), and to reproduce the observed range of SN Ia luminosities. Successful models have been produced by several groups employing a variety of mechanisms (Nomoto, Thielemann, & Yokoi 1984; Livne 1990; Khokhlov, Müller, & Höflich 1993; Woosley & Weaver 1994; Höflich, Khokhlov, & Wheeler 1995). Although the details of the explosion mechanism remain an active area for research, many plausible (but similar) models match the spectral features of SN Ia, and can produce the relation between light curve shape and luminosity detected by P93.

The local sample of SN Ia shows that the light curve shapes and luminosities are weakly correlated with the type of galaxy in which they occur (H96a). Spirals show a wide range of light curve shapes while ellipticals show a narrow range. If left untreated, the relation between stellar population and the luminosities of SN Ia could poison the inference of cosmological parameters by introducing a subtle drift in SN Ia properties with look-back time (von Hippel, Bothun, & Schommer 1997). We know that the rate of SN Ia per unit B luminosity is almost twice as high in spirals as in ellipticals at the present epoch (Cappellaro et al. 1997). If we assume this increased rate of SN Ia production is related to the higher rate of star formation in spirals, then the SN Ia in spirals come from progenitors which are likely to be younger than the progenitors of SN Ia in ellipticals. Incidentally, this is the conclusion reached by Oemler and Tinsley (1979) nearly two decades ago.

However, our local sample calibrates the effect. Figure 3 shows that the calibration of RPK96, which does not use any information about galaxy type as an input, results in distances to early-type (8 objects) and late-type galaxies (19 objects) which are consistent to 0.006 ± 0.07 magnitudes (SN Ia with elliptical hosts give slightly closer distances). To obtain limits on the possible offsets between SN Ia with early-type and late-type progenitors,

we perform a Monte Carlo simulation with the following assumptions. Late-type galaxies have SN Ia with young and old progenitors at a ratio of 1:1 (a conservative limit from their rates — spirals have twice the rate of supernovae as ellipticals, so 1/2 of the progenitors are old and 1/2 are young), and ellipticals contain only old progenitors. Simulated data sets demonstrate that with the above assumptions, and the observed offsets between distances to ellipticals and spirals, the allowed range in the distance offsets between objects with young and old progenitors is 0.02 ± 0.15 mag. If the ratio of young to old progenitors in spirals were to be 2:1, then the limits become 0.01 ± 0.11 mag. This unsophisticated analysis, while not providing hard limits on evolution, demonstrates there is no obvious dependence on SN Ia distances with respect to the age of the stellar population in which they reside. Since, at $z = 0.5$, we still expect to see SN Ia originating from a mixture of young and old progenitors, the average evolution should be smaller than the maximum possible differences quoted above. A larger sample of objects and a better understanding of the local rates as a function of progenitor type, as will be provided by the Mount Stromlo Abell Cluster Supernova Search (Reiss et al. 1998), will increase the power of this type of test.

Theory provides another avenue by which to explore the possible effects of evolution. Höflich, Thielemann & Wheeler(1997) have calculate the differences in light curve shape, luminosity, and spectral characteristics of SN Ia as a function of the initial composition and metallicity of their white dwarf progenitors. Their calculations show that although changes in restframe U can be considerable, the effects in the B and V bands are only ~ 0.05 mags, even when considerable changes are made to the metallicity and C/O ratio of the white dwarf progenitors. Changes to the light curve shapes of the objects may also occur, and in total their calculations suggest distances could drift by as much as 0.3 mag in B and 0.15 mag in V . At what redshift such differences could appear is unclear, but these types of changes would be accompanied by significant spectral differences, and should not go undetected.

We assume that the relation between light curve shape and luminosity that holds for a wide range of stellar populations at low redshift also covers the range of stellar populations we encounter in our high-redshift sample. The range of ages for SN Ia progenitors in the nearby sample is likely to be larger than the look-back time to the galaxies in our high-redshift sample, so we expect that our local calibration will work well at eliminating any pernicious drift in the supernova distances between the local and distant samples. Although we expect this approach to be valid for joining our nearby and distant samples, until we know more about the stellar ancestors of SN Ia, we need to be vigilant for changes in the properties of the SN at significant look-back times. These might be detected as changes in the spectra or colors of SN Ia with redshift.

5.4. Selection Biases

Like every sample selected by a flux limit, our SN Ia sample will be affected by the shift of the mean to intrinsically brighter objects near our redshift limit due to the dispersion of their intrinsic luminosities; this is often referred to as Malmquist bias (e.g., Gonzalez & Faber 1997). Generally speaking, the bias is proportional to σ^2 of the distance indicator. Since we only suffer the bias left *after* the correction for light curve shape, the average bias is much smaller than for uncorrected SN Ia peak brightnesses. This is fortunate, because it is not a straightforward task to correct for luminosity biases in the limited sample of objects produced by a particular SN search.

In addition to classic Malmquist bias, the SN Ia we discover at high redshift are subject to a number of selection effects. These could affect the average properties of our sample as a function of redshift, and could possibly bias our measurement of the (D_L, z) relation. The supernovae discovered by the High-Z SN Search are limited by their detectability between two epochs (typically 25 days apart in the observer’s frame), and only those

objects which increase in flux by an amount greater than our detection threshold are discovered. Therefore, our ability to discover a supernova depends not only on its brightness at maximum light, but also on its age, the light curve shape of the object, and redshift due to time dilation of the light curves.

We have performed Monte Carlo simulations in which we randomly explode SN Ia assuming their rate is constant with look-back time, identifying which objects would be discovered in a search by our supernova program. These simulations show that with SN Ia distances of precision $\sigma = 0.15$ mag, our average measurement of Ω_M will be biased high by ~ 0.05 for $0 < \Omega_M < 1$ ($\Omega_\Lambda = 0$). Though it may seem surprising, selection biases are significantly less than other sources of error, such as the uncertainty in $(B - V)$, because the scatter in luminosity, after correction for light curve shape, is so small. Nevertheless, selection effects are a source of systemic error that should be removed.

Corrections could be computed through Monte Carlo simulations for equation (6) provided that the selection function (completeness vs. magnitude) for finding objects were known. Unfortunately, the selection function for discovering SN Ia is not sharply defined; it depends critically on the PSF of both the pre-discovery and discovery images, and our procedure ultimately rests on a human decision of whether an object is real. Since false detections waste scarce observing time, observers are reluctant to follow the light curve of an object unless the probability the object is real is very high. Perlmutter et al. (1997) performed simulations to determine the magnitude limit for each of their discovery frames, adding stars to galaxies and then measuring their ability to recover them in software. Our experience with similar simulations is that our software selects fainter objects than human reviewers will accept as being real. By comparing Monte Carlo simulations of the expected redshift distribution of objects to the actual sample, it should be possible to estimate corrections to these detection thresholds.

Rather than apply corrections to individual objects, it would be better to employ a maximum likelihood approach in which one finds the most likely cosmological model, given the SN redshifts, estimated detection thresholds, SN distances and light curves, and detection simulations. This is an involved, computationally expensive procedure, which is probably not yet warranted given the small size of the corrections and the limited set of data.

5.5. Weak Gravitational Lensing

It has been pointed out by Kantowski, Vaughan, & Branch (1995) that large-scale structure could magnify (or demagnify) a SN’s light through weak gravitational lensing as it travels to an observer. Wambsganss et al. (1997) have computed the effect for Ω_Λ -dominated and Ω_M -dominated flat universes, and find that weak lensing could produce a modest increase in the dispersion of a distance indicator (approximately 5% at $z = 1$). It also leads to a small systematic shift in observed SN brightnesses to fainter magnitudes — approximately 1% at $z = 1$. The average line-of-sight to a SN is more likely to pass through voids than clusters and filaments, leading to an average demagnification. Holz and Wald (1997) have calculated a “worst case” scenario for the effect of gravitational lensing, where the universe’s mass is made up of randomly distributed objects with mass greater than $0.01M_\odot$. At $z = 0.5$ for $\Omega_M = 1$, an average standard candle is made 0.15 mag fainter by the lensing. The effect is more pronounced at $z \approx 1$, and is diminished as Ω_M approaches 0, as suggested by the SN observations presented here, by Garnavich et al. (1998), and by Perlmutter et al. (1998). Given the size of other systematic errors, uncertainties due to gravitational lensing are not likely to be of major concern up to $z \approx 1$. It is unlikely that we might find an event which has undergone significant lensing so that it can be readily separated from the intrinsic dispersion of SN Ia brightnesses, although Kolatt & Bartelmann

(1998) suggest how to maximize these events by searching through galaxy clusters.

5.6. Summary of Uncertainties

The data presented by Garnavich et al. (1998) and Riess et al. (1998) indicate that we can measure the distances to high- z supernovae with a statistical uncertainty of $\sigma = 0.2$ mag (10%) per object. With only 10 objects a comparison of $z \approx 0$ and $z \approx 0.5$ can be made to a precision of better than 5% — leaving systematic uncertainties as a major contributor to the total error budget. A summary of the contributions to high-redshift supernova distance uncertainties is given in Table 1. This table shows that our program to measure cosmology will most likely be limited by the possibility of the evolution of SN Ia explosions with look-back time. Future work to address this possible problem will be as important as obtaining large numbers of objects at high redshift.

6. Observations and Analysis of SN 1995K

6.1. Photometry and Spectroscopy

In 1995 February and March our team imaged approximately 2.5 square degrees with the CTIO 4 m telescope + 2048² CCD. Our first attempts at searching for supernovae in these data were hampered by distortions caused by curvature in the CCD, and general inexperience. However, in an image taken on 30 March (UT dates are used throughout this paper), a new object was discovered in a galaxy at position (J2000.0) $\alpha = 10^h 50^m 47^s.0$, $\delta = -09^\circ 15' 07''.4$ (Figure 5). This object was reported to the IAU and designated SN 1995K (Schmidt et al. 1995).

We obtained spectra of SN 1995K using the ESO NTT+EMMI on 1995 April 3. CCD

images containing the SN spectra were bias subtracted, and the spectrum of the object extracted as a single pixel row, to minimize the contribution of the host galaxy. The spectra were then wavelength calibrated with comparison lamp spectra interspersed with the SN observations, and the resulting individual spectra were combined. The extracted host galaxy spectrum was scaled and subtracted. The host galaxy’s redshift, measured from its H α emission, is $z = 0.479$. The spectrum was binned to increase the S/N ratio per resolution element, and the resulting spectrum is plotted in Figure 6. Also plotted is the spectrum of SN 1994D (Filippenko 1997) near maximum light, binned to the same resolution as SN 1995K. The spectrum of SN 1995K appears to be typical of SN Ia, exhibiting the characteristic Si II absorption at a rest wavelength of $\lambda 6150 \text{ \AA}$ and is incompatible with peculiar SN Ia such as SN 1991T (Filippenko et al. 1992a; Phillips et al. 1992; Ruiz-Lapuente et al. 1992; Ford et al. 1993) or SN 1991bg (Filippenko et al. 1992b; Leibundgut et al. 1993; Turatto et al. 1996). Using the spectral aging technique of Riess et al. (1997), we estimate the age of the SN on this date, 1995 April 3, to be 1 ± 2 days past maximum light, *independent* of, and in agreement with its light curve. An additional spectrum of SN 1995K’s host galaxy was obtained on 1995 Apr 25 with the CTIO 4 m telescope (Figure 6). Comparison of the galaxy spectrum with the catalog of Kennicutt (1992) shows this galaxy to be consistent with a star-forming galaxy of type Sb/c.

CCD images of SN 1995K were obtained at several telescopes in $B45$ and $V45$ filters, and in some cases R_C and I_C . The sequence of stars shown in Figure 7 was calibrated on three photometric nights by observing spectrophotometric standards listed in Appendix A and standards of [Landolt (1992a) for R_C and I_C measurements], measuring the color and extinction transformation coefficients, and applying these to observations of the SN 1995K field. The resulting magnitudes were averaged from multiple nights and are given in Table 2, with uncertainties calculated from the dispersion of the observations. Relative photometry between the supernova and the stellar sequence was carried out as prescribed in §4.3, using

a template for galaxy subtraction obtained with the CTIO 4 m+2048² CCD on 1996 March 15. SN 1995K’s light curve was brought to the standard system by offsetting from the standard star sequence, and applying color corrections derived for each instrumental setup (these corrections ranged from -0.01 to 0.04 mag per mag of $(B_{45} - V_{45})$). The resulting light curve is listed in Table 3.

6.2. The Luminosity Distance to SN 1995K

The K-corrections to translate B_{45} and V_{45} observations of SN Ia at a redshift of $z = 0.479$ to restframe B and V , respectively, are plotted in Figure 8. The K-corrections are nearly constant, because of the close match of these redshifted filters to their restframe counterparts. Table 4 lists each corrected photometric measurement, the time-dilated age of the SN with respect to maximum fit from the light curve (iteratively determined by applying K-corrections, fitting the light curve, and refitting the K-corrections, until convergence occurs), and the resulting restframe magnitudes for SN 1995K. The light curve of SN 1995K has already successfully been used to provide strong evidence for the predicted effects of time dilation (Leibundgut et al. 1996) in SN light curves (Leibundgut 1990).

The light curve of SN 1995K is plotted in Figure 9, and is of sufficient quality to provide an accurate luminosity distance to its $z = 0.479$ host. Using the techniques described in H95 we derive $\Delta m_{15}(B) = 1.15 \pm 0.1$ mag for SN 1995K, and restframe brightnesses at maximum light of $m_B = 22.93 \pm 0.08$ mag and $m_V = 23.04 \pm 0.13$ mag. This decline rate and color at maximum are typical for the unreddened SN Ia we observe in the nearby Universe. The derived distance modulus, applying the $\Delta m_{15}(B)$ versus M_V relations of H96a (their Table 3), is $(m - M)_V = 42.31 \pm 0.13$ mag, and the Hubble diagram which includes SN 1995K and the H96b distance measurements to 29 objects is shown in Figure 10. Applying MLCS (RPK96) to SN 1995K indicates that this SN is slightly over-luminous relative to

the average ($\Delta = 0.07$), is unreddened, and has a distance modulus of 42.40 ± 0.25 mag on the RPK96 scale. This object and the distance measurements of RPK96 are plotted in Figure 11. Distances derived to the nearby and distant supernovae must be done in exactly the same manner, so the results of these two ways of using the light curve shape are not plotted on the same diagram. However, one can compare the resulting (D_L, z) relation, and the bottom halves of Figures 10 and 11 demonstrate that a consistent result is obtained.

With a single object it is difficult to make serious conclusions about cosmological parameters, regardless of the distance precision it offers, because there is no way to judge systematic errors in an empirical way. However, taken at face value, if $\Omega_\Lambda = 0$, SN 1995K yields an estimate for the matter density of the Universe to be $\Omega_M = -0.2_{-0.8}^{+1.0}$, where we have taken the range to include both the H96 and RPK96 distance uncertainties, extinction uncertainties, and uncertainties due the sources of systematic error described in §5. For a spatially flat universe composed of normal matter and a cosmological constant, we find $\Omega_M = 0.4_{-0.4}^{+0.5}$, $\Omega_\Lambda = 0.6_{-0.5}^{+0.4}$. An $\Omega = \Omega_M = 1$ universe is excluded with greater than 80% confidence from this single distance estimate.

Perlmutter et al. (1997) present luminosity distances to 7 high-redshift supernovae. Direct comparison with our work is difficult, because not all of their objects were positively identified as SN Ia (two of their objects have decline rates more extreme than any other known SN Ia and do not have confirming spectra), and their single-color results cannot be corrected for extinction in the host galaxy. However, taken on equal terms, SN 1995K suggests that Ω_M may be lower than the central value of $\Omega_M = 0.88_{-0.60}^{+0.69}$ they find. Recent *HST* observations by the two groups (Garnavich et al. 1998; Perlmutter et al. 1998) seem to confirm this view, yielding values of $\Omega_M = -0.1 \pm 0.5$ and $\Omega_M = 0.2 \pm 0.4$, respectively. More data will elevate this discussion.

7. The Future

SN 1995K is the first of more than 30 confirmed SN Ia discovered by the High-Z SN Search (Schmidt et al. 1995, 1997a, 1997b; Kirshner et al. 1995; Suntzeff et al. 1996; Garnavich et al. 1996a,b, 1997a,b). The observations presented here indicate that these objects, and those of Perlmutter et al. (1997), should provide an accurate method of tracing out luminosity distances to high redshifts. Figure 12 shows the level of precision likely to be achieved by a sample of N SN Ia with observations of comparable precision to those of SN 1995K; a measurement of Ω_M to ± 0.2 should be achieved from objects at $z = 0.5$ given our expected systematic uncertainties. The High-Z SN Search has been allocated sufficient orbits to follow about 8 SN Ia with the *HST* in two photometric bands. We have already obtained observations of three SN Ia, one of which lies at $z = 0.97$ (Garnavich et al. 1998). As demonstrated in Figure 2, this object lies in a window in which it would be possible to obtain accurate restframe B and V observations of SN Ia with *HST*. A sample of 10 such $z = 1$ objects, coupled with the $z = 0.5$ sample, would provide enough information to separate the individual effects of Ω_M and Ω_Λ (Goobar & Perlmutter 1995). Figure 13 shows the 1σ joint confidence region for Ω_M and Ω_Λ that is obtainable with a sample of 30 SN Ia observed at $z = 0.5$ augmented with 10 SN Ia observed at $z = 1$ with *HST*. As can be seen from the figure, although Ω_M and Ω_Λ are not individually measured accurately, the combination $\Omega_M - \Omega_\Lambda$ is tightly constrained. If we limit ourselves to flat cosmological models, $\Omega_M + \Omega_\Lambda = 1$, the uncertainty in Ω_M and Ω_Λ would become small, with uncertainties in each quantity of approximately 0.1.

Although measurements of the CMB anisotropy on small scales still have several years to reach maturity, the high- z SN Ia and CMB observations are complementary. The error ellipses of these two measurements in the $(\Omega_M, \Omega_\Lambda)$ plane will be nearly perpendicular to each other (Figure 13). When combined, they could provide a definitive measurement of

the global parameters of our Universe.

We wish to thank Ed Carter at NOAO for tracing the redshifted filter set. AVF acknowledges support from NSF grant AST-9417213. RPK acknowledges support from NSF grants AST-9528899 and AST-9617058, and thanks the Institute for Theoretical Physics, University of California, Santa Barbara for their generous hospitality. AGR acknowledges support from the Miller Institute for Basic Research in Science, University of California, Berkeley. SN research at UW is supported by the NSF and NASA. CWS acknowledges the generous support of the Seaver Institute and the Packard Foundation. MH acknowledges support provided for this work by the NSF through grant number GF-1002-97 from the Association of Universities for Research in Astronomy, Inc., under NSF Cooperative Agreement No. AST-8947990 and from Fundación Andes under project C-12984; MH also acknowledges support by Cátedra Presidencial de Ciencias 1996-1997. Partial support for AC was provided by the NSF through grant GF-1001-95 from AURA, Inc., under NSF cooperative agreement AST-8947990, and from Fundación Antorchas Argentina under project A-13313. This research used IRAF, an astronomical reduction package distributed by the National Optical Astronomy Observatories, which is operated by the Association of Universities for Research in Astronomy, Inc. (AURA) under cooperative agreement with the NSF.

REFERENCES

- Arnett, W. D. 1969, *Ap&SS*, 5, 280
- Barbon, R., Rosino, L., & Iijima, T. 1989, *A&A*, 220, 83
- Baum, W.A. 1957, *AJ*, 62, 6
- Bessell, M.S. 1990, *PASP*, 102, 1181
- Bouchet, P., Lequeux, J., Maurice, E., Prevot, L., Prevot-Burnichon, M.L., 1985, *A&A*, 149, 330.
- Branch, D. 1987, *ApJ*, 316, 81L
- Branch, D., Fisher, A., Baron, E., & Nugent, P. 1996, *ApJ*, 470, L7
- Branch, D., & Miller, D.L. 1993, *ApJ*, 405, L5
- Cappellaro, E. et al. 1997, *A&A*, 322, 431
- Coles, P., & Lucchin, F. 1995, “Cosmology” (John Wiley & Sons: Chicester), pp. 31-46
- Cousins, A.W.J. 1980, *MNSSA*, 39, 93
- Colgate, S., & McKee, W., 1969, *ApJ*, 157, 623
- Evans, R. 1994, *PASAu*, 11, 7
- Filippenko, A. V. 1997, *ARAA*, 35, 309
- Filippenko, A. V., et al. 1992a, *ApJ*, 384, L15
- Filippenko, A. V., et al. 1992b, *AJ*, 104, 1543
- Fisher, A., Branch, D., Höflich, P., & Khokhlov, A. 1995, *ApJ*, 447, L73
- Ford, C. H., Herbst, W., Richmond, M.W., Baker, M.L., Filippenko, A.V., Treffers, R.R., Paik, Y., & Benson, P.J. 1993, *AJ*, 106, 1101
- Garnavich, P., et al. 1996a, *IAUC* 6332

- Garnavich, P., et al. 1996b, IAUC 6358
- Garnavich, P., et al. 1997a, IAUC 6633
- Garnavich, P. et al. 1998b, ApJ, 000, L000
- Gonzalez, A. H., & Faber, S. M. 1997, ApJ, 485, 80
- Goobar, A., & Perlmutter S. 1995, ApJ, 450, 14
- Groth, E.J. 1986, AJ, 91, 1244
- Guerra, E.J., & Daly, R. A. 1998, ApJ, 493, 536
- Gunn, J.E. 1978 in *Observational Cosmology: The 8th Advanced Course of the Swiss Society of Astronomy and Astrophysics*, ed. A Maeder, L. Martinet, & G. Tammann (Saverny: Geneva), p 1.
- Hamuy, M., et al. 1993a, AJ, 106, 2392
- Hamuy, M., Phillips, M. M., Wells, L. A., & Maza, J. 1993b, PASP, 105, 787
- Hamuy et al. 1994, AJ, 108, 2226
- Hamuy, M., Phillips, M.M., Maza, J., Suntzeff, N.B., Schommer, R.A., & Avilés, R. 1995, AJ, 109, 1 [H95]
- Hamuy, M., Phillips, M.M., Schommer, R.A., Suntzeff, N.B., Maza, J., & Avilés, R. 1996, AJ, 112, 2391 [H96a]
- Hamuy, M., Phillips, M.M., Suntzeff, N.B., Schommer, R.A., Maza, J., & Avilés, R. 1996, AJ, 112, 2398 [H96b]
- Hamuy, M., et al. 1996, AJ, 112, 2408 [H96c]
- Hamuy, M., Phillips, M.M., Suntzeff, N.B., Schommer, R.A., Maza, J., Smith, R.C., Lira, P., & Avilés, R. 1996, AJ, 112, 2438 [H96d]
- Höflich, P., Khokhlov, A., & Wheeler, J.C. 1995, ApJ, 444, 831

- Höflich, P., Wheeler, J.C., & Thielemann, F. K. 1998, *ApJ*, 495, 617
- Holz, D. E., Wald, R. M., 1998, astro-ph/9708036
- Hoyle, F., & Fowler, W.A. 1960, *ApJ*, 132, 565
- Hu, W. 1996, in *The Universe at High z, Large-Scale Structure, and the Cosmic Microwave Background*, ed. E. Martnez-Gonzlez & J. L. Sanz (Berlin: Springer), 207
- Humason, M.L., Mayall, N.U., & Sandage, A.R. 1956, *ApJ*, 61, 97
- Kantowski, R., Vaughan, T., & Branch, D. 1995, *ApJ*, 447, 35
- Kellerman, K.I., 1993, *Nature*, 361, 134
- Kennicutt, R.C., 1992, *ApJS*, 79, 255
- Khokhlov, A., Müller, E., & Höflich, P. 1993, *A&A*, 270, 223
- Kirshner, R. P., et al. 1995, IAUC No. 6267
- Kim, A., Goobar, A., & Perlmutter, S. 1996, *PASP*, 108, 190
- Kim, A., et al. 1997, *ApJ*, 483, 565
- Kolatt, T.S., & Bartelmann, M. 1998 *MNRAS*, submitted astro-ph/9708120
- Kowal, C. T. 1968, *AJ*, 73, 1021
- Landolt, A. U. 1992a, *AJ*, 104, 340
- Landolt, A. U. 1992b, *AJ*, 104, 372
- Lauer, T., & Postman, M. 1992, *ApJ*, 400, 47
- Leibundgut, B. 1990, *A&A*, 229, 1
- Leibundgut, B., & Spyromilio, J. 1997 in *The Early Universe with the VLT*, ed. J. Bergeron, (Berlin: Springer), 95
- Leibundgut, B., et al. 1993, *AJ*, 105, 301

- Leibundgut, B., et al. 1996, ApJ, 466, L21
- Lira, P. 1996, M.S. thesis, Universidad de Chile
- Livne, E. 1990, ApJ, 354, L53
- McNaught, R. H. 1990, IAUC 5039
- Martin, R., Williams, A., & Woodings, S. 1997, IAUC 6558
- Mattig, W. 1958, Astr.Nach., 184, 109
- Minkowski, R. 1960, ApJ, 132, 908
- Mueller, J. 1989, IAUC 4920
- Nomoto, K., Thielemann, F., & Yokoi, K. 1984, ApJ, 286, 644
- Nørgaard-Nielsen, H. U., et al. 1989, Nature, 339, 523
- Oemler, A., & Tinsley, B. M. 1979, AJ, 84, 985
- Oke, J.B., & Sandage, A. 1968, ApJ, 154, 21
- Oke, J.B., Hoessel, J. E., & Gunn, J. G. 1996, AJ, 111, 29
- Peebles, P. J. E. 1993, “Principles Of Physical Cosmology”, Princeton University Press,
Princeton, New Jersey
- Perlmutter, S., et al. 1992 in “Robotic Telescopes in the 1990s” ed. A.V. Filippenko (San
Francisco: ASP Conf. Ser. 34), p. 67
- Perlmutter, S., et al. 1995, ApJ, 440, L41
- Perlmutter, S., et al. 1997, ApJ, 483, 565
- Perlmutter, S., et al. 1998, Nature, 391, 51 (Erratum: 392, 311)
- Phillips, A.C., & Davis, L.E. 1995 “Astronomical Data Analysis Software and Systems”, ed.
R.A. Shaw, H.E. Payne, & J.J.E. Hayes (San Francisco: ASP Conf. Ser. 77), p. 297

- Phillips, M. M., Wells, L.A., Suntzeff, N.B., Hamuy, M., Leibundgut, B., Kirshner, R. P., & Foltz, C.B. 1992, AJ, 103, 1632
- Phillips, M. M. 1993, ApJ, 413, L105 [P93]
- Phillips, M. M., et al. 1998, in preparation
- Phillips, M. M., et al. 1987, PASP, 99, 592
- Pollas, C. 1992, IAUC 5420
- Reiss, D., Germany, L., Schmidt, B. P., & Stubbs, C. 1998, AJ, 115, 26.
- Riess, A.G., Press, W. H., & Kirshner, R. P. 1995, ApJ, 438, L17 [RPK95]
- Riess, A.G., Press, W. H., & Kirshner, R. P. 1996a, ApJ, 473, 88 [RPK96]
- Riess, A.G., Press, W. H., & Kirshner, R. P. 1996b, ApJ, 473, 588
- Riess, A.G., et al. 1997, AJ, 114, 722
- Riess, A.G., et al. 1998, AJ submitted
- Robertson, H.P. 1936, ApJ, 83, 187
- Ruiz-Lapuente, P., Cappellaro, E., Turatto, M., Gouiffes, C., Danziger, I.J., Della Valle, M., & Lucy, L.B. 1992, ApJ, 387, L33
- Rhoads, J. E. 1997, submitted to ApJ astro-ph/9705163
- Saha, A., Sandage, A., Labhardt, L., Tammann, G. A., Macchetto, F. D., & Panagia, N. 1997, ApJ, 486, 1
- Sandage, A.R., 1961, ApJ, 133, 355
- Sandage, A., & Tammann, G.A. 1993, ApJ, 415, 1
- Schechter, P.L., Mateo, M., & Saha, A. 1993, PASP, 105, 1342
- Schmidt, B. P. 1997, in “Thermonuclear Supernovae”, ed. P. Ruiz-Lapuente, R. Canal, & J. Isern (Dordrecht: Kluwer), p. 765

- Schmidt, B., et al. 1995, IAUC 6160
- Schmidt, B., et al. 1996, BAAS, 28, 1420
- Schmidt, B., et al. 1997a, IAUC 6602
- Schmidt, B., et al. 1997b, IAUC 6646
- Shanks, T., et al. 1984, MNRAS, 206, 767
- Stepanas, P.G., & Saha, P. 1995, MNRAS, 272, L13
- Stetson, P. B. 1987, PASP, 99, 191
- Suntzeff, N.B., et al. 1996, IAUC 6490
- Tammann, G.A., & Leibundgut, B. 1990, A&A, 236, 9
- Tammann, G.A., & Sandage, A. 1995, ApJ, 452, 16
- Tinsley, B. 1972, ApJ, 178, 319
- Treffers, R., Leibundgut, B., Filippenko, A.V., & Richmond, M. W. 1993, BAAS, 25, 834
- Turatto, M., et al. 1996, MNRAS, 283, 1
- van den Bergh, S. 1995, ApJ, 453, L55
- van den Bergh, S., & Pazder, J. 1992, ApJ, 390, 34
- von Hippel, T., Bothun, G. D., & Schommer, R.A. 1997, AJ, 114, 1154
- Walker, A.G. 1936, Proc. Lond. Math. Soc., 42, 90
- Wambsganss, J., Cen, R., Guohong, X., & Ostriker, J. 1997, ApJ, 475, L81
- Weinberg, S. 1972, Gravitation and Cosmology: Principles and Applications of the General
Theory of Relativity (John Wiley & Sons: New York)
- Wheeler, J.C., & Harkness R. P. 1990, Rep. Prog. Phys. 53, 1467
- Woosley, S. E., & Weaver, T.A. 1994, ApJ, 423, 371

Yoshi, Y., & Peterson, B. A. 1995, ApJ, 444, 15

Zaldarriaga, M., Spergel, D.N., & Seljak, U. 1997, ApJ, 488, 1

Zwicky, F. 1968, PASP, 80, 462

A. Appendix: The High-Z Standard System

We have created a new set of broadband filters which represent the Johnson B and V filters redshifted to $z = 0.35$ and $z = 0.45$. We call these $B35$, $V35$, $B45$, and $V45$, respectively. Traces of each filter have been supplied by the manufacturer, *Omega Optical*, and these traces have been verified at KPNO using a spectrophotometer. The sensitivity functions S_{B35} , S_{V35} , S_{B45} , and S_{V45} of our broadband filters have been derived by combining these filter traces with a quantum efficiency curve of a thinned SITE CCD and a normalized function which increases linearly with λ (Table 5). This latter function is included because CCDs are photon detectors and standard sensitivity functions (e.g., Bessell 1990) assume that a star with spectrum F_λ in filter i has magnitude m_i given by

$$m_i = -2.5 \log \frac{\int S_i(\lambda) F_\lambda(\lambda) d\lambda}{\int S_i(\lambda) d\lambda} + \mathcal{Z}_i. \quad (\text{A1})$$

For the purposes of the High-Z SN Search, the exact definition of our zero points \mathcal{Z}_i is not important. As long as we use a consistent method in our calculations with equations (12) and (10), our derived K-corrections are sensitive only to the difference in zero points between our redshifted filters and the Johnson filters, e.g. $\mathcal{Z}_B - \mathcal{Z}_{B45}$. Rather than establishing our standard system’s zero point using Vega, we use the Hamuy et al. (1994) spectrophotometric standards. These stars have accurate broadband photometry in the standard systems of Cousins (1980) and Landolt (1992b), the systems with which our nearby supernova observations have been calibrated. This consistency is important because our program’s goal is to make as accurate a differential measurement as possible of SN brightnesses as function of redshift.

We define \mathcal{Z}_i of our broadband filters such that A-type stars with $(V - I) = 0$ mag have $B35 = V35 = B45 = V45 \equiv V$. Hamuy et al. (1994) have observed a set of A-type stars (referred to as secondary standards) which have $V - I_C \approx 0$. Since the Hamuy stars do not have exactly $V - I_C = 0$, we must apply small corrections to m_V of the stars to

obtain magnitudes in our filter system. We use equation (A1) to derive the magnitudes of the tertiary stars of Hamuy et al. (1994), which have $-0.3 < (V - I_C) < 0.8$, in our bandpasses, and then obtain the linear transformation between our system and the Johnson/Kron-Cousins systems of the form

$$m_i = a_{ij}(V - I_C) + m_j. \quad (\text{A2})$$

The transformations used to convert the Johnson/Kron-Cousins system to our new system are listed in Table 7 and the fits shown in Figure (14). We use these values to transform the secondary standards of Hamuy to the high-redshift SN system, and these stars and their derived magnitudes are listed as the first 10 stars in Table 6. Because of the near zero color of the Hamuy secondary stars, the corrections, even for the $B35$ and $V35$ filters which have large transformation coefficients, are very small (< 0.02 mag). We compute the \mathcal{Z}_i for our filters by comparing the magnitudes for the Hamuy secondary stars obtained from equation (A2) with the magnitudes obtained from equation (A1), and adjusting \mathcal{Z}_i for each filter so that the average offset between the two sets of magnitudes is zero. The resulting \mathcal{Z}_i are given in Table 7. Table 6 lists the $B35, V35, B45, V45$ magnitudes of the Hamuy tertiary stars using these \mathcal{Z}_i with equation (A1). The Hamuy secondary and tertiary stars form the primary standards for the high-redshift SN photometric system. In a future paper we will present observations of these standard stars and use them to calibrate selected Landolt (1992a) fields.

Fig. 1.— The differences in the (D_L, z) relation for various cosmological models expressed as the difference in distance modulus from an empty Universe, $\Omega = 0$.

Fig. 2.— The uncertainty in transforming to restframe B (top) and V (bottom) as a function of redshift for V , R_C , and I_C , *HST* 850LP (WFPC) and 110M (NICMOS), and the $B35$, $V35$, $B45$, and $V45$ filters described in Appendix A.

Fig. 3.— The residual of SN Ia distances from RPK96 plotted as a function of galaxy type. The offset between the early-type and late-type galaxies is 0.006 ± 0.07 mag.

Fig. 4.— The magnitude at maximum of a typical SN Ia as a function of redshift for as observed in R_C and I_C for $\Omega_M = \Omega = 0$.

Fig. 5.— The template image of SN 1995K taken 1995 March 7, the discovery image of SN 1995K taken 1995 Mar 30, and the resulting subtracted image obtained as described in §4.2.

Fig. 6.— The spectrum of SN 1995K obtained with the ESO NTT on 1995 April 3 (UT), compared to that of SN Ia 1994D (Filippenko 1997) near maximum light. The spectra have been binned to the same resolution, and the good match indicates SN 1995K is a SN Ia caught near peak brightness. Also shown is the spectrum of SN 1995K’s host galaxy as obtained on 1995 Apr 25 with the CTIO 4 m telescope.

Fig. 7.— The field around SN 1995K as observed by the CTIO 4 m telescope, with the position of the SN and photometric sequence stars marked.

Fig. 8.— The measured K-corrections for individual spectra plotted as a function of supernova age for transforming $V45$ to V (top) and $B45$ to B (bottom) for SN Ia at $z = 0.479$. A fifth-order polynomial is fit to the data.

Fig. 9.— The restframe B (bottom) and V (top) light curves of SN 1995K. The data are

K-corrected and time-dilated, and the RPK96 (solid line) and H95 (dotted line) fits are superposed.

Fig. 10.— A Hubble diagram containing SN 1995K using the distances and techniques of H96b(top), and these distances plotted as a residual in distance modulus ($m - M$), with respect to an empty ($\Omega = 0$) Universe.

Fig. 11.— A Hubble Diagram containing SN 1995K using the distances and techniques of RPK96 (top), and these distances plotted as a residual in distance modulus ($m - M$), with respect to an empty ($\Omega = 0$) universe.

Fig. 12.— The uncertainty in $\Omega = \Omega_M$ as a function of the sample size for objects with observations similar to SN 1995K observed at $z = 0.5$. Four cases of systematic error are considered [$\sigma_{sys} = 0.0, 0.05$ (expected), 0.10 mag, and 0.20 mag] and are plotted as separate lines in the figure.

Fig. 13.— Predicted error contours (68.3% and 95.4% joint confidence) in measuring Ω_M and Ω_Λ simultaneously for a sample of 30 $z = 0.5$ SN Ia augmented with 10 $z = 1$ SN Ia observed with *HST*. The underlying cosmology in the simulation is $\Omega_M = 0.4, \Omega_\Lambda = 0$. Also shown, as dotted lines, are the predicted uncertainty contours (68.3% and 95.4% confidence) from future CMB anisotropy measurements to be made by the Planck Surveyor mission (Zaldarriaga, Spergel, & Seljak 1997).

Fig. 14.— $(B35 - V)$, $(B45 - R_C)$, $(V35 - I_C)$, and $(V45 - I_C)$ plotted as a function of $(V - I_C)$. The best fitting linear transformation is superposed as given in Table 6.

Table 1. Summary of Error Contributions to High Supernova Distances

Systematic Uncertainties(1σ)	(mag)	Statistical Uncertainties	(mag)
Photometric System Zero Point ^a	0.05	Individual Zero Points	0.02
Selection Effects	0.02	Shot noise	0.15
Evolution	< 0.17	K-corrections	0.03
Evolution of Extinction Law	0.02	Extinction	0.10
Gravitational Lensing	0.02	σ of SN Ia	0.15

^aIncludes propagated effect on extinction, $3.1\sigma E(B - V)$.

Table 2. A Photometric Sequence Near SN 1995K

Star	B45	V45	R	I
1	21.72(03)	20.91(04)	21.66(03)	20.85(04)
2	20.06(01)	19.60(01)	20.03(02)	19.57(03)
3	17.05(01)	16.40(01)	17.01(02)	16.36(02)
4	20.51(02)	18.88(04)	20.40(03)	18.77(04)
5	17.28(02)	16.51(03)	17.22(03)	16.45(04)
6	17.18(02)	16.83(03)	17.15(03)	16.80(04)
7	20.72(03)	20.31(03)	20.69(04)	20.28(05)
8	19.75(02)	19.40(03)	19.73(03)	19.37(03)
9	18.16(02)	17.72(03)	18.13(03)	17.69(03)
10	20.64(04)	19.11(03)	20.53(04)	19.01(03)
11	18.57(02)	17.60(02)	18.50(02)	17.54(03)
12	19.83(02)	19.46(03)	19.81(03)	19.44(03)
13	19.63(02)	17.99(03)	19.52(03)	17.88(03)

Note. — Uncertainties in hundredths of a magnitude are listed in parentheses.

Table 3. Photometric Data for SN 1995K

JD	Date	B45	V45	R	I	Telescope	Observer
2449774.6	1995 Feb 26	>24.5	CTIO 4m	Hamuy et al.
2449783.6	1995 Mar 07	24.09(38)	CTIO 4m	Hamuy et al.
2449801.7	1995 Mar 25	22.26(15)	CTIO 4m	Hamuy et al.
2449806.6	1995 Mar 30	22.19(06)	CTIO 4m	Hamuy et al.
2449810.6	1995 Apr 03	...	22.02(30)	22.37(12)	...	ESO NTT	Leibundgut & Spyromilio
2449812.6	1995 Apr 05	22.28(15)	...	ESO 3.6m	Walsh
2449812.6	1995 Apr 05	22.23(09)	22.18(10)	LCO 2.4m	Dressler
2449814.7	1995 Apr 07	22.44(14)	22.25(15)	LCO 2.4m	Dressler
2449815.6	1995 Apr 08	22.39(12)	22.48(22)	LCO 2.4m	Dressler
2449815.7	1995 Apr 08	22.64(14)	22.36(14)	KPNO 4m	Ciardullo
2449816.6	1995 Apr 09	22.62(12)	22.48(12)	LCO 2.4m	Dressler
2449817.5	1995 Apr 10	22.79(12)	LCO 2.4m	Dressler
2449830.6	1995 Apr 23	23.62(30)	22.95(30)	ESO NTT	Leibundgut
2449831.5	1995 Apr 24	23.70(25) ^a	22.95(30) ^b	ESO NTT	Leibundgut
2449836.5	1995 Apr 29	23.96(33)	22.92(29)	ESO 1.5m	Leibundgut
2449866.4	1995 May 29	>24.30	>23.50	ESO NTT	Spyromilio

Note. — Uncertainties in hundredths of a magnitude are listed in parentheses.

^aGunn-*r*.

^bGunn-*i*.

Table 4. The Light Curve of SN 1995K Corrected to the Restframe

JD	age(days)	B	V	K_B	K_V
2449774.6	-20.8	> 25.23	...	-0.73	...
2449783.6	-14.7	24.82(38)	...	-0.73	...
2449801.7	-2.4	23.01(15)	...	-0.75	...
2449806.6	0.9	22.94(06)	...	-0.75	...
2449810.6	3.6	23.11(12)	22.87(30)	-0.74	-0.85
2449812.6	4.9	23.02(15)	...	-0.74	...
2449812.6	4.9	22.96(09)	23.02(10)	-0.73	-0.84
2449814.7	6.4	23.18(14)	23.09(15)	-0.74	-0.84
2449815.6	7.0	23.13(12)	23.32(22)	-0.74	-0.84
2449815.7	7.0	23.36(14)	23.22(14)	-0.72	-0.86
2449816.6	7.6	23.35(12)	23.32(12)	-0.73	-0.84
2449817.5	8.2	23.53(12)	...	-0.74	...
2449830.6	17.1	24.34(28)	23.78(27)	-0.72	-0.83
2449831.5	17.7	24.43(25)	23.72(30)	-0.73	-0.77
2449836.5	21.1	24.69(33)	23.74(29)	-0.73	-0.82
2449866.4	41.3	> 25.02	> 24.31	-0.72	-0.81

Note. — Uncertainties in hundredths of a magnitude are listed in parentheses.

Table 5. Sensitivity Functions of the High-Z Filter Set

Wavelength(\AA)	$S_\lambda(\text{B35})$	$S_\lambda(\text{B45})$	$S_\lambda(\text{V35})$	$S_\lambda(\text{V45})$
5100.0	0.002	0.000	0.000	0.000
5200.0	0.246	0.000	0.000	0.000
5300.0	0.708	0.000	0.000	0.000
5400.0	0.923	0.000	0.000	0.000
5500.0	0.996	0.000	0.000	0.000
5600.0	1.000	0.127	0.000	0.000
5700.0	0.987	0.628	0.000	0.000
5800.0	0.953	0.933	0.000	0.000
5900.0	0.904	0.930	0.000	0.000
6000.0	0.938	0.962	0.000	0.000
6100.0	0.964	0.987	0.000	0.000
6200.0	0.884	0.909	0.000	0.000
6300.0	0.878	0.944	0.000	0.000
6400.0	0.924	1.000	0.000	0.000
6500.0	0.864	0.934	0.000	0.000
6600.0	0.702	0.917	0.128	0.000
6700.0	0.440	0.927	0.606	0.000
6800.0	0.237	0.887	0.868	0.000
6900.0	0.121	0.857	0.950	0.000
7000.0	0.064	0.795	0.965	0.000
7100.0	0.041	0.573	1.000	0.080
7200.0	0.027	0.330	0.962	0.329
7300.0	0.017	0.180	0.892	0.649

Table 5—Continued

Wavelength(\AA)	$S_{\lambda}(\text{B35})$	$S_{\lambda}(\text{B45})$	$S_{\lambda}(\text{V35})$	$S_{\lambda}(\text{V45})$
7400.0	0.013	0.095	0.861	0.860
7500.0	0.009	0.055	0.837	0.978
7600.0	0.007	0.036	0.817	1.000
7700.0	0.004	0.023	0.832	0.952
7800.0	0.002	0.017	0.849	0.908
7900.0	0.000	0.013	0.814	0.882
8000.0	0.000	0.011	0.578	0.855
8100.0	0.000	0.000	0.323	0.849
8200.0	0.000	0.000	0.168	0.829
8300.0	0.000	0.000	0.088	0.719
8400.0	0.000	0.000	0.048	0.500
8500.0	0.000	0.000	0.029	0.312
8600.0	0.000	0.000	0.018	0.171
8700.0	0.000	0.000	0.012	0.097
8800.0	0.000	0.000	0.009	0.054
8900.0	0.000	0.000	0.006	0.034
9000.0	0.000	0.000	0.005	0.021
9100.0	0.000	0.000	0.003	0.014
9200.0	0.000	0.000	0.002	0.009
9300.0	0.000	0.000	0.001	0.006
9400.0	0.000	0.000	0.000	0.003
9500.0	0.000	0.000	0.000	0.001

Table 6. Primary Standards for the High-Z Standard System

Star Name ^a	B35	B45	V35	V45
HR718	4.285	4.299	4.329	4.340
HR1544	4.352	4.344	4.340	4.333
HR3454	4.346	4.378	4.448	4.480
HR4468	4.711	4.721	4.749	4.760
HR4963	4.373	4.369	4.373	4.370
HR5501	5.699	5.696	5.699	5.699
HR7596	5.583	5.548	5.499	5.473
HR7950	3.765	3.761	3.764	3.764
HR8634	3.428	3.439	3.474	3.489
HR9087	5.147	5.163	5.207	5.228
L377	11.077	10.947	10.750	10.656
L1020	11.335	11.180	10.938	10.820
EG21	11.431	11.468	11.513	11.536
L1788	12.991	12.854	12.636	12.527
L2415	12.074	11.955	11.761	11.662
H600	10.380	10.326	10.245	10.200
L3218	11.818	11.776	11.698	11.662
L3864	12.009	11.870	11.649	11.539
L4364	11.435	11.362	11.266	11.221
F56	11.072	11.085	11.126	11.141
L4816	13.787	13.791	13.770	13.758
CD32	10.365	10.290	10.185	10.135
L6248	11.638	11.493	11.261	11.147

Table 6—Continued

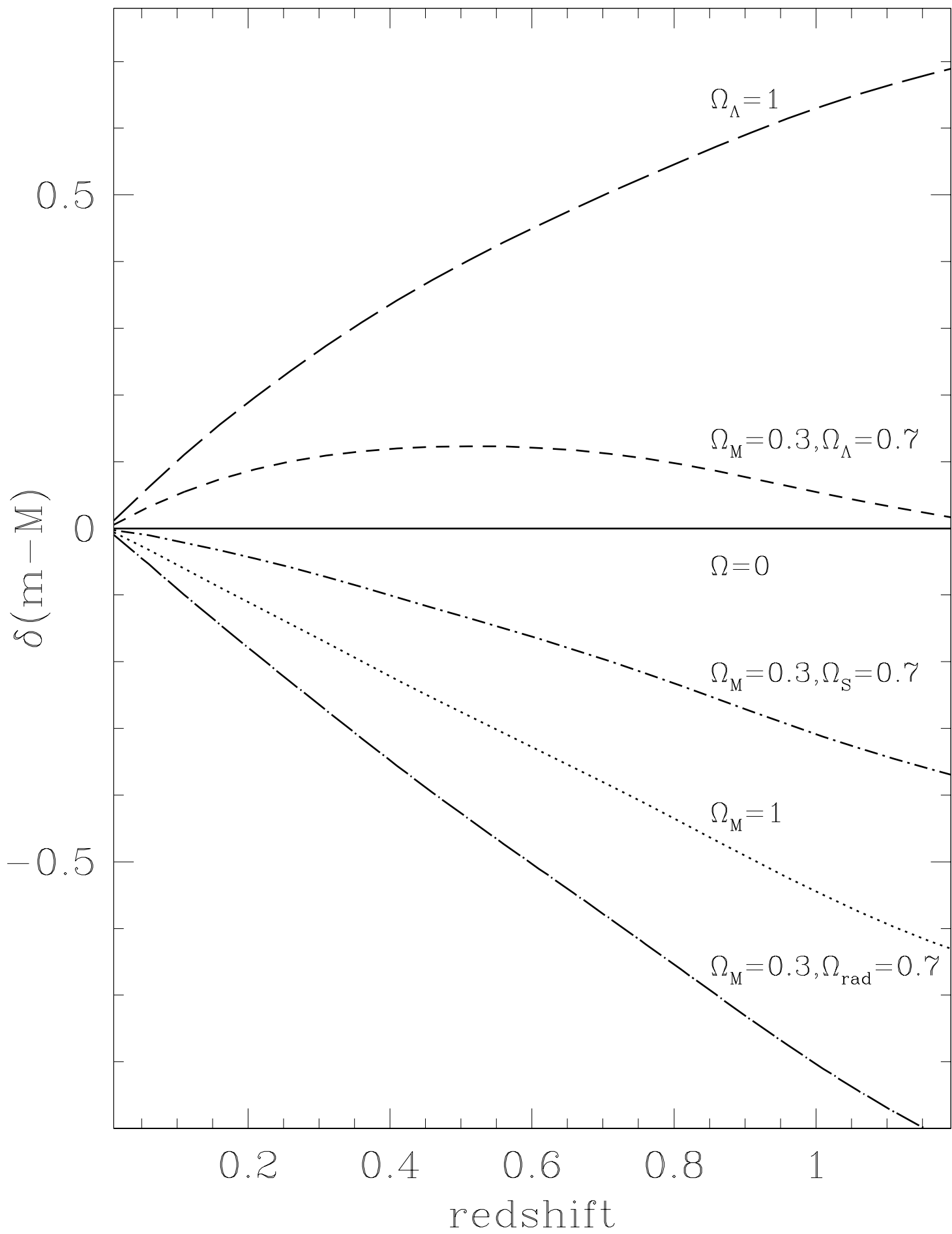
Star Name ^a	B35	B45	V35	V45
EG274	11.093	11.140	11.215	11.258
L7379	10.048	9.892	9.656	9.543
L7987	12.278	12.311	12.350	12.372
L9239	11.876	11.711	11.452	11.326
F110	11.893	11.957	12.081	12.138
L9491	14.093	14.067	14.043	14.037

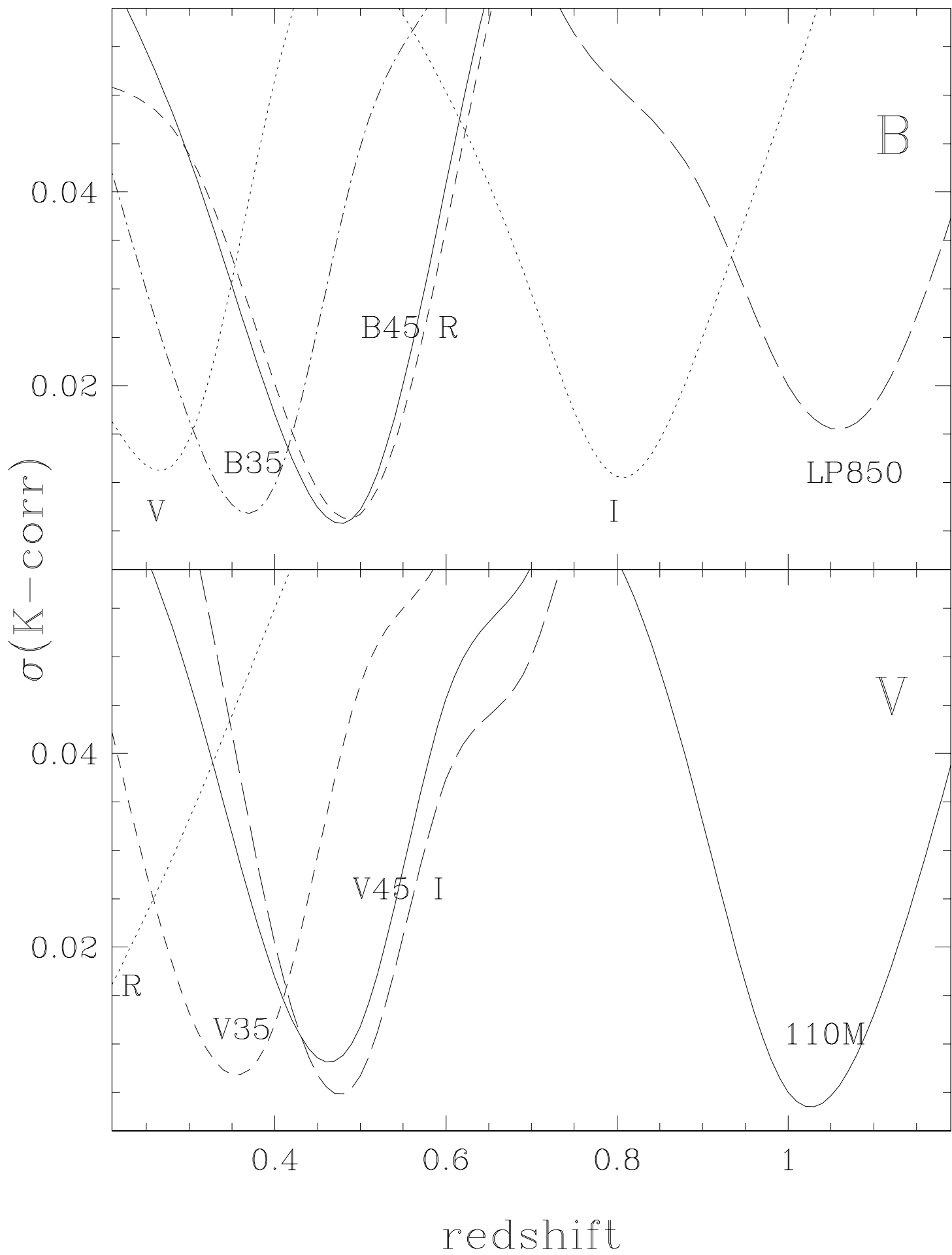
^aAs listed in Hamuy et al. (1992).

Table 7. The High-Z Filter System Transformations and Zero Points

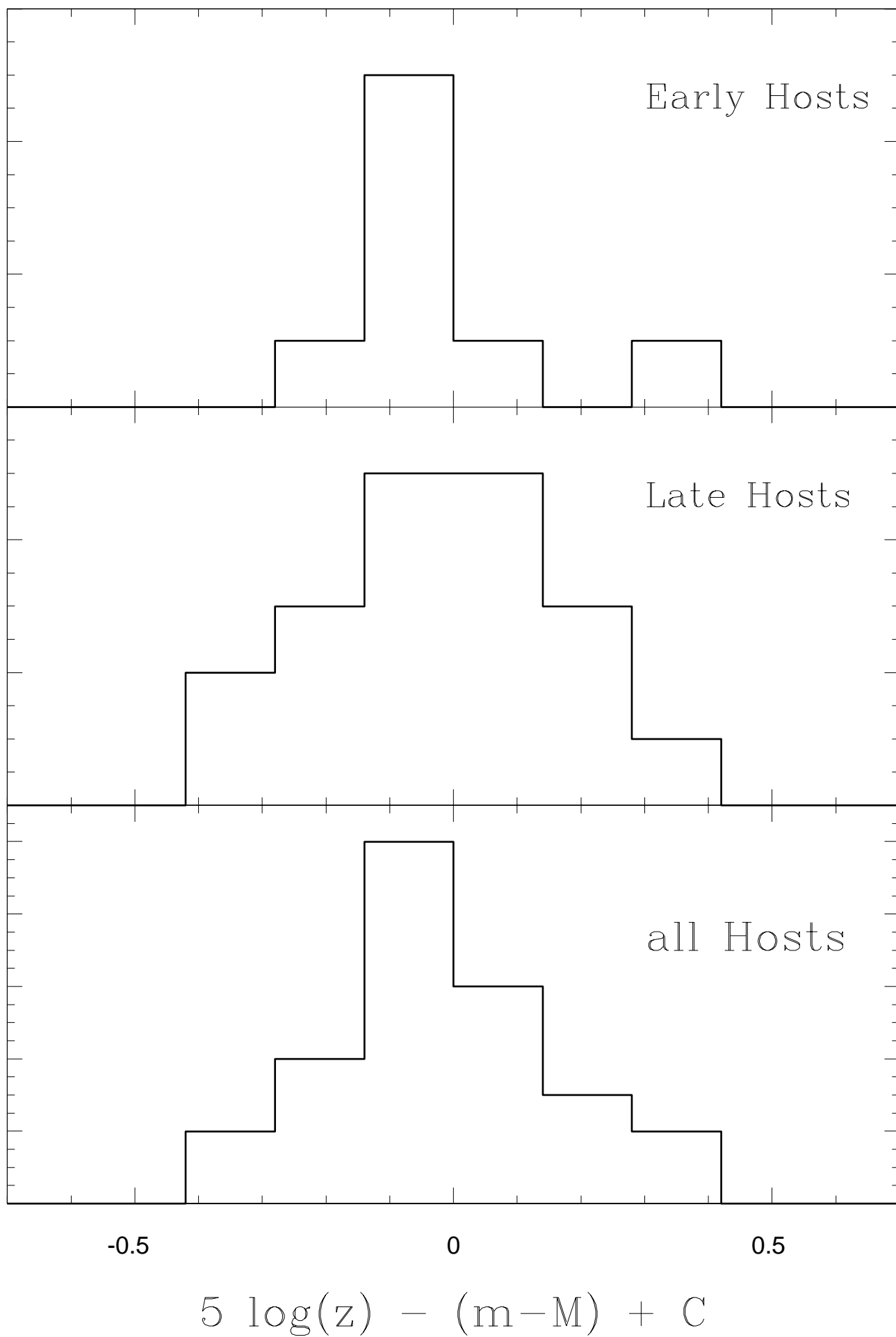
Transformation	Zero Point ^a
$B35 = -0.246(V - I_C) + V$	ZP= -21.339
$B45 = +0.027(V - I_C) + R_C$	ZP= -21.582
$V35 = +0.198(V - I_C) + I_C$	ZP= -22.045
$V45 = +0.034(V - I_C) + I_C$	ZP= -22.292

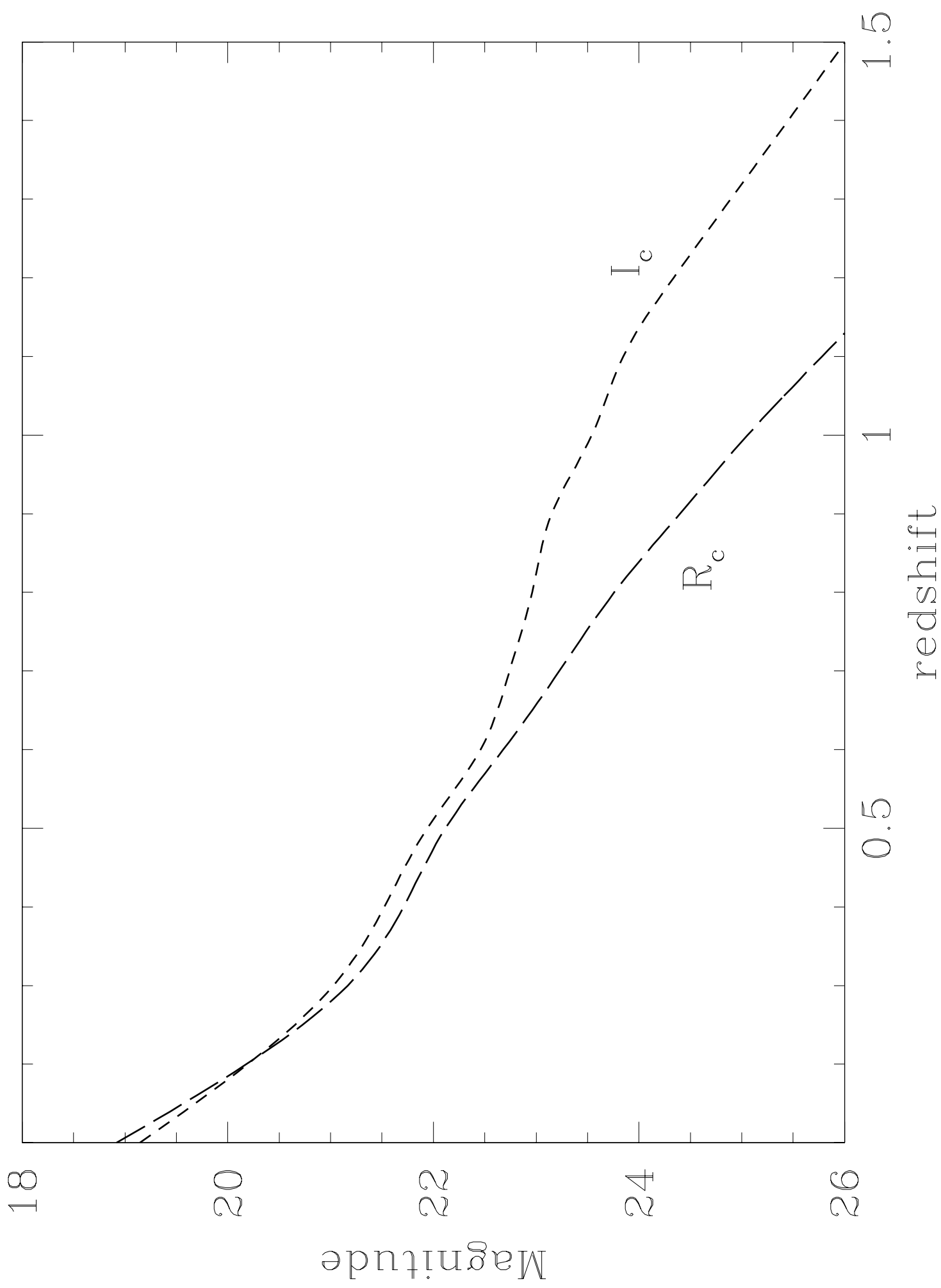
^aZero Point required for equation (10) if F_λ is in units of $\text{ergs cm}^{-2} \text{s}^{-1} \text{\AA}^{-1}$.





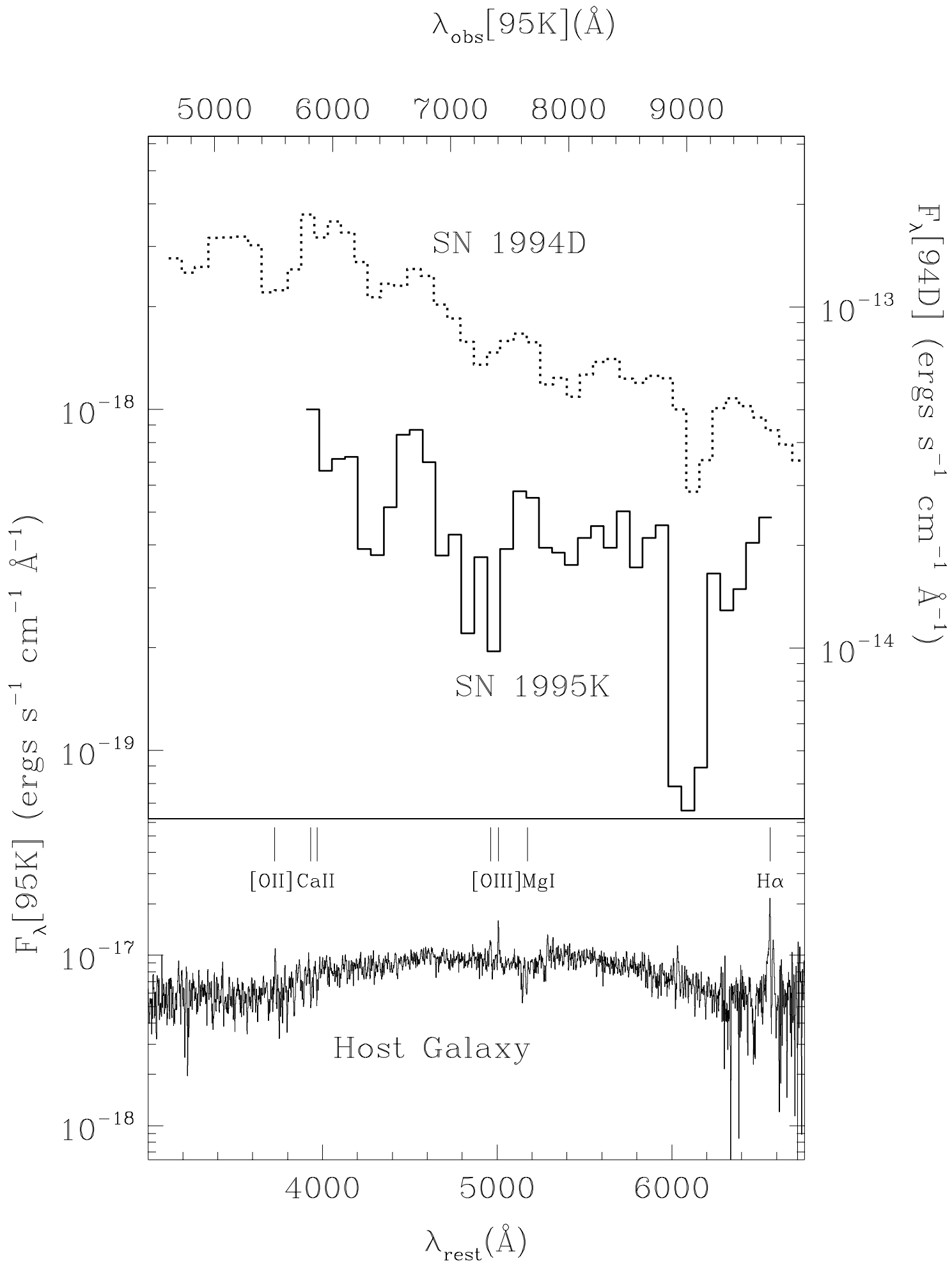
Number of SN Ia





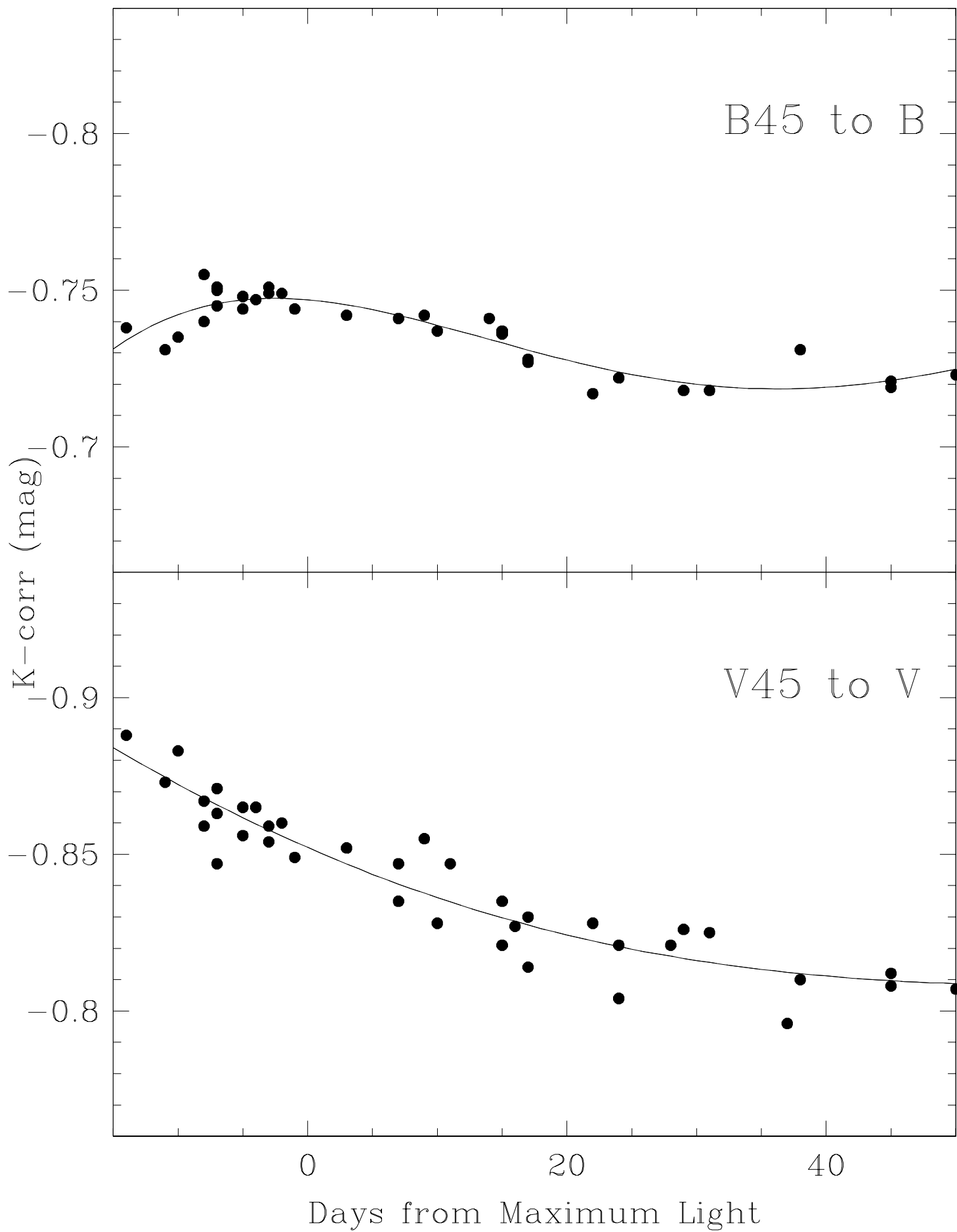
This figure "fig5.gif" is available in "gif" format from:

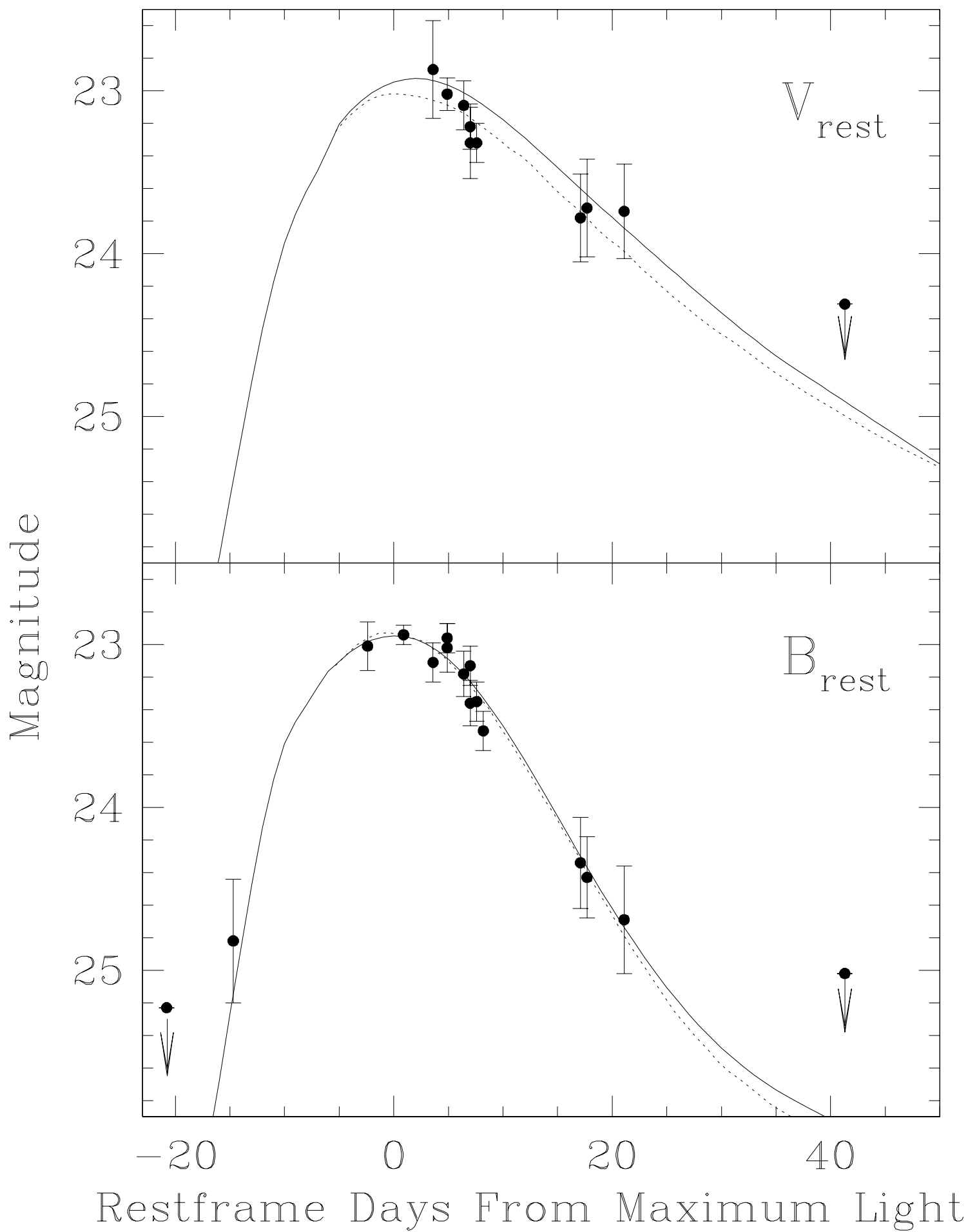
<http://arXiv.org/ps/astro-ph/9805200v1>



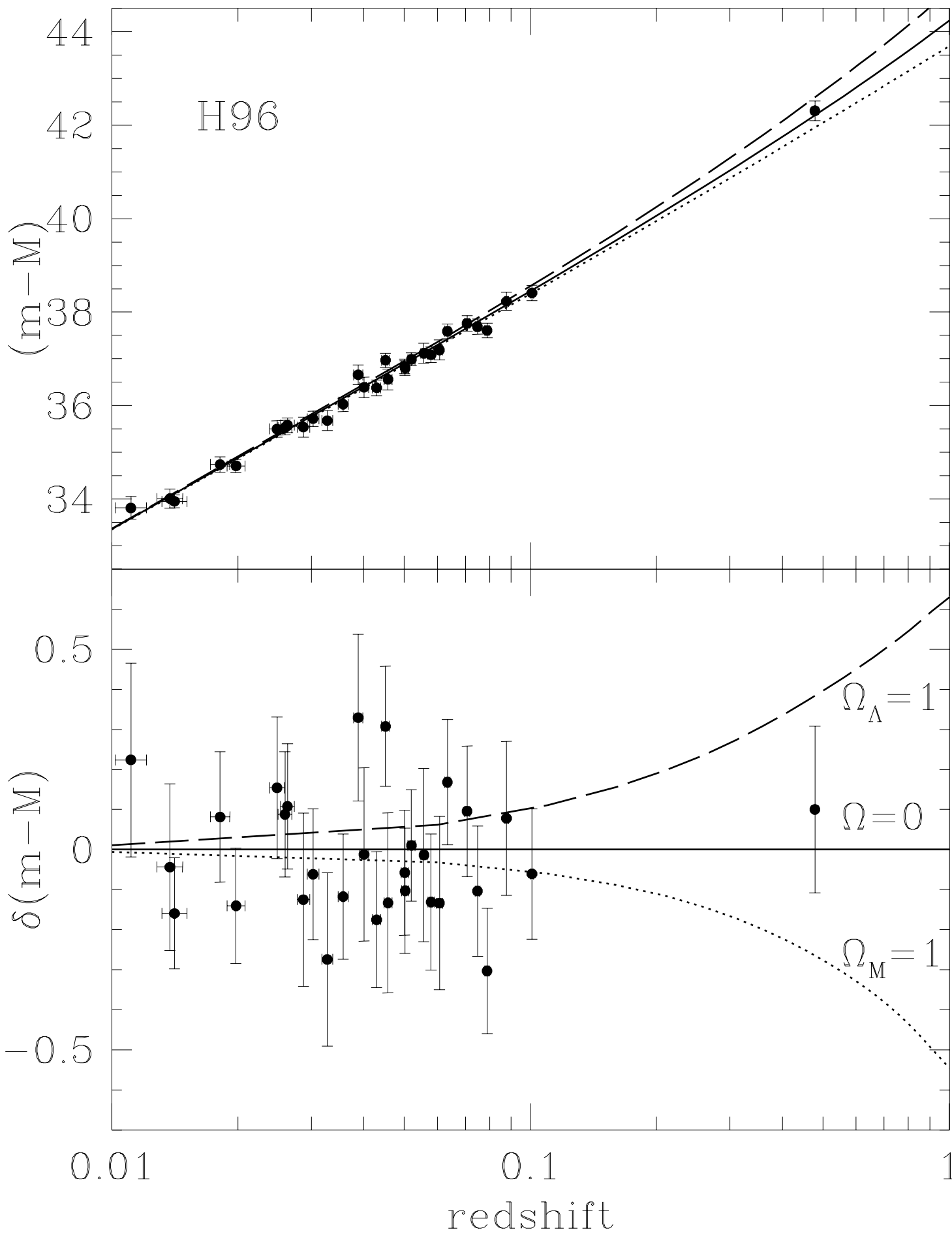
This figure "fig7.gif" is available in "gif" format from:

<http://arXiv.org/ps/astro-ph/9805200v1>





H96



RPK96

